2017-08-01

Role of Molecular Chaperonin CCT and Its Co-Chaperone PhLP1 in the Assembly of mTOR Complexes

Madhura Vinayak Dhavale
Brigham Young University

Role of Molecular Chaperonin CCT and Its Co-Chaperone PhLP1 in the Assembly of mTOR Complexes

Madhura Vinayak Dhavale

A dissertation submitted to the faculty of
Brigham Young University
in partial fulfillment of the requirements for the degree of

Doctor of Philosophy

Barry M. Willardson, Chair
Joshua L. Andersen
Kenneth A. Christensen
John C. Price
Michael R. Stark

Department of Chemistry and Biochemistry

Brigham Young University

ABSTRACT

Role of Molecular Chaperonin CCT and Its Co-Chaperone PhLP1
in the Assembly of mTOR Complexes

Madhura Vinayak Dhavale
Department of Chemistry and Biochemistry, BYU
Doctor of Philosophy

mTOR is the central kinase in biochemical pathways that regulate cellular growth, protein synthesis and cell survival. Deregulation of mTOR signaling results in uncontrolled cell proliferation and hence is implicated in various cancers and autoimmune diseases. mTOR functions through two distinct signaling complexes, called mTORC1 and mTORC2. CCT is a cytosolic chaperonin that assists in folding of several protein substrates. In these studies, we have identified two components of the mTOR complexes, mLST8 and Raptor, as substrates of CCT. We have performed biochemical and signaling studies which indicate that CCT is involved in assembly and signaling of mTOR complexes by folding β-propeller domains of mLST8 and Raptor. We have also obtained high resolution structural information of the mLST8-CCT complex by cryo-EM and mass spectrometric cross-linking. Moreover, we have explored the role of PhLP1 as a co-chaperone for CCT in the assembly of mTOR complexes. Interestingly, we found that PhLP1 plays very different roles in the case of mLST8 and Raptor. While PhLP1 participate in assembly of mLST8 into mTOR complexes, it facilitates degradation of Raptor. These biochemical data, combined with structural information, can be used to design small molecules that modulate mTOR signaling by affecting the formation of intact mTOR complexes.

Keywords: [mTOR, mLST8, Raptor, CCT, cryo-EM, Chaperones]

ACKNOWLEDGEMENTS

I am grateful to the department of Chemistry and Biochemistry for giving me this opportunity to work as a graduate student and provide financial support. I am thankful to Dr. Willardson for his insightful mentorship and moral support during the tough phases of my research work. I want to thank my past colleague Dr. Takuma Aoba and present colleagues Nicole Tensmeyer and Grant Ludlam for their contribution to these studies. This study would not be complete without the help of our collaborators Jose M. Valpuesta from Centro Nacional de Biotecnología in Madrid and Sarah Franklin from University of Utah. Last but not the least; I want to appreciate my family for their constant emotional support.

TABLE OF CONTENTS

LIST OF FIGURES

ABBREVIATIONS

2D	two dimensional
3D	three dimensional
40S	eukaryotic small ribosomal subunit
4EBP	eukaryotic translation factor 4E binding protein
ADP	adenosine diphosphate
AGC group	group of protein kinases including PKA, PKG, and PKC
AKT	Ak virus strain thymoma protein, also called protein kinase B
AMPK	adenosine monophosphate kinase
ATM	ataxia telangiectasia mutated
ATP	adenosine triphosphate
ATR	ataxia- and Rad3-related
β-propeller	protein tertiary structure motif of 4-8 β-sheets that form a toroid
BzF	p-benzoyl-L-phenylalanine
C-terminus	amino acids at the protein carboxyl terminus
Cas9	CRISPR associated protein 9
CCT	chaperonin containing tailless polypeptide 1, also called TRiC
cDNA	complementary DNA
CHAPS	3-[(3-cholamidopropyl)dimethylammonio]-1-propanesulfonate
c-Myc	avian myelocytomatosis virus oncogene cellular homolog
CRIM	conserved domain in middle
CRISPR	clustered regularly interspaced short palindromic repeats
DEP	Dishevelled EGL10 and pleckstrin
DEPTOR	DEP domain-containing mTOR-interacting protein
DNA	deoxyribonucleic acid
DNA-PKcs	DNA-dependent protein kinase catalytic subunit
DSG	disuccinimidyl glutetate
DSS	disuccinimidyl suberate
DTT	dithiothreitol

EDTA	ethylenediaminetetraacetic acid
eEF	eukaryotic translation elongation factor
eIF	eukaryotic translation initiation factor
EM	electron microscopy
ERK	extracellular signal-required kinase
FAT	FRAP, ATM, TRRAP
FATC	FAT domain at C-terminus
FBS	fetal bovine serum
FKBP	FK 506 binding protein
FRB	FKBP-Rapamycin binding
G protein	guanine nucleotide binding signaling protein
GAPDH	glyceraldehyde 3-phosphate dehydrogenase
GβL	Gβ-like, also called mLST8
GFP	green fluorescent protein
Gβ	G protein β subunit
Gγ	G protein γ subunit
GPCR	G protein coupled receptor
GRB10	Growth factor receptor-bound protein 10
GSK3β	glycogen synthase kinase 3 β
GTP	guanosine triphosphate
GTPase	enzyme that hydrolyzes GTP to GDP
HA	hemagglutinin
HEAT	Huntingtin, EF3A, ATM, TOR
HEK	human embryonic kidney
HEPES	4-(2-hydroxyethyl)-1-piperazineethanesulfonic acid
HEPG2	liver hepatocellular carcinoma
His_6	hexahistidine
HPC4	Ca^{2+}-dependent protein C epitope
HSP	heatshock protein
IGF	insulin-like growth factor
IRS1	Insulin –receptor substrate 1
KD	kinase domain
LBE	LST binding element

LC-MS/MS	liquid chromatography followed by tandem mass spectrometry
LTQ	linear ion trap quadrupole
MG132	Benzyl N-[(2S)-4-methyl-1-[[(2S)-4-methyl-1-[[(2S)-4-methyl-1-oxopentan-2-yl]amino]-1-oxopentan-2-yl]amino]-1-oxopentan-2-yl]carbamate
mLST8	mammalian lethal with Sec13 protein 8
MS	mass spectrometry
mSIN1	mammalian stress-activated protein kinase interacting protein 1
mTOR	mechanistic target of rapamycin
mTORC	mTOR complex
N-Myc	v-myc avian myelocytomatosis viral oncogene neuroblastoma derived homolog
NP-40	nonyl phenoxypolyethoxylethanol
NTD	N-terminal domain
p53	cellular tumor antigen p53
PAGE	polyacrylamide gel electrophoresis
PBS	phosphate buffered saline
PDCD5	programmed cell death 5
PDK1	3-phosphoinositide dependent protein kinase-1
PDZ	postsynaptic density of 95 kDa, Discs large and zonula occludens 1
PEI	polyethylenimine
PH	pleckstrin homology
PhLP1	phosducin-like protein 1
PI3K	phosphatidylinositol 3-kinase
PIKK	phosphatidylinositol 3-kinase-related kinases
PIP2	phosphatidylinositol 4,5-bisphosphate
PIP3	phosphatidylinositol (3,4,5)-trisphosphate
PKCα	protein kinase C alpha
PMSF	phenylmethane sulfonyl fluoride or phenylmethylsulfonyl fluoride
PRAS40	proline-rich Akt substrate of 40 kDa
PROTOR	Protein observed with Rictor
PTEN	phosphatase and tensin homolog
Rag	Ras-related GTPase
Raptor	regulatory associated protein of mTOR
Ras	rat sarcoma

RBD	ribosome binding domain
RBD	Ras-binding domain
REDD1	regulated in development and DNA damage responses 1
Rheb	Ras homolog enriched in brain
Rictor	rapamycin-insensitive companion of mTOR
RNA	ribonucleic acid
RNC	Raptor N-terminal conserved
S6	ribosomal protein S6
S6K	S6 kinase
SAIN	Shc and IRS-1 NPXY binding
SDS	sodium dodecyl sulfate
SEC	size exclusion column
SGK	serum/glucocorticoid regulated kinase 1
sgRNA	small guide RNA
siRNA	small interference RNA
SMG1	suppressor of morphogenesis in genitalia
TEV	tobacco etch virus
TFA	trifluoroacetic acid
TOS	TOR signaling
TRD	tetratricopeptide repeats
TSC	tuberous sclerosis complex
TTT-R2TP	Tel2-Til1-Til2 and Rvb1/2-Tah1-Pih1
ULK1	unc 51-like autophagy activating kinase 1
VHL	von Hippel Lindau tumor repressor
WAC	WW domain containing adaptor with coiled-coil
WD40	protein primary sequence motif of 40 amino acids often ending in WD, successive WD40 repeats create β-propeller structures
XL-MS	chemical crosslinking coupled with mass spectrometry

CHAPTER 1 : INTRODUCTION TO MTOR SIGNALING

1.1 Summary

The mTOR (mechanistic target of Rapamycin) kinase is the central metabolic regulator that promotes cell growth and inhibits autophagy. mTOR responds to various signals like amino acids, glucose, insulin, and redox status, exerting its effects through two structurally and functionally distinct complexes called mTORC1 and mTORC2. The mTORC1 core complex contains additional subunits called mLST8 and Raptor, whereas the mTORC2 core complex contains mLST8, Rictor and mSIN1 subunits. The mLST8 subunit stabilizes the mTOR kinase, and Raptor and Rictor recruit specific substrates to the kinase. In contrast, mSIN1 confers phosphatidylinositol 3,4,5 trisphosphate sensitivity to the mTORC2 complex.

Misregulation of mTOR signaling can lead to uncontrolled cell division and hence is implicated in different types of cancers. mTOR signaling can be controlled by manipulating folding and assembly of the structural components of mTOR complexes. Folding of the mTOR kinase by the HSP90/TTT/R2TP chaperone machinery has been extensively studied. However, detailed information about the folding of the other mTORC components is not yet available. Previously, our lab has studied the folding of the β subunit of the G-protein heterotrimer (Gβ) by the cytosolic chaperonin CCT and its co-chaperone PhLP1. mLST8 is also called Gβ-like due to its structural similarity to Gβ. Both mLST8 and Gβ contain WD-40 repeat sequences with characteristic β-propeller structural folds that are also found in several other substrates of CCT. These facts led us to investigate the possibility that CCT and PhLP1 are chaperones for mLST8 and two other WD40 repeats containing mTOR components, namely Raptor and Rictor.

1.2 Introduction

1.2.1 mTOR signaling

The mechanistic target of Rapamycin (mTOR) kinase is a master regulator of cell proliferation, metabolism, and survival. The mTOR kinase responds to extracellular stimuli including growth hormones such as insulin and nutrients such as amino acids, or intracellular stimuli such as redox potential. mTOR controls key biochemical processes like protein and lipid synthesis, glucose metabolism and autophagy, thereby regulating cell size, cell division, and cell longevity. mTOR derives its name from Rapamycin, an antifungal agent produced by a soil bacterium called Streptomyces hygroscopius first discovered on the South Pacific Island of Rapa Nui (Easter Island). When rapamycin enters the cell, it forms a complex with peptide prolyl isomerase FKBP12, which then acts as an inhibitor of mTOR. Defects in mTOR signaling are implicated in different cancers, diabetes, and aging, thus making it a valuable therapeutic target. Several Rapamycin analogs (Rapalogs) and other mTOR inhibitors are currently being used as immunosuppressants and anti-cancer drugs.

1.2.2 mTORC1 and mTORC2

mTOR signals through two distinct complexes, called mTOR complex 1 (mTORC1) and mTOR complex 2 (mTORC2). Both the mTOR complexes have mTOR as the central kinase and some accessory components that are unique to mTORC1 and mTORC2. These accessory components assist mTOR in substrate recognition or provide a scaffold for protein-protein interactions. They also determine subcellular localization of mTOR. mTORC1 consists of three core components – mTOR, mLST8 (mammalian lethal with Sec 13 protein 8), and Raptor

(Regulatory protein associated with TOR) (Figure 1.1). Additionally, mTORC1 contains two non-core components – PRAS 40 (Proline-rich AKT substrate of 40 kDa) and DEPTOR (Dep domain containing mTOR-interacting protein) [1].

mTORC2 consists of four core components, namely mTOR, mLST8, Rictor (Rapamycin-insensitive companion of mTOR), and mSIN1 (mammalian stress-activated protein kinase interacting protein 1) (Figure 1.1). mTORC2 also contains two non-core components, namely DEPTOR and PROTOR 1/2. Due to unique structural and functional components, mTORC1 and 2 are different with regard to Rapamycin sensitivity, physiological roles, and cellular localization. Acute Rapamycin treatment inhibits mTORC1 whereas mTORC2 inhibition requires prolonged Rapamycin treatment for inhibition [2]. In a comparative study of muscle-specific Raptor and Rictor knockout mice, only Raptor knockouts showed severe muscle dystrophy, indicating that mTORC1 is critical for muscle function. mTORC1 and mTORC2 play different roles in glucose homeostasis in adipocytes [3]. For example, adipocyte-specific Raptor knockout mice showed enhanced glucose tolerance, protection against diet-induced obesity and leaner body type, whereas Rictor knockouts in adipocytes resulted in high insulin resistance, deficient glucose metabolism and accumulation of fats in skeletal muscles [4]. mTORC1 is primarily present in the cytosol and lysosomal vesicles while mTORC2 is found in plasma membrane and cytoplasm [5-7]. Raptor and Rictor bind to mTOR in a mutually exclusive manner to determine its fate [8].

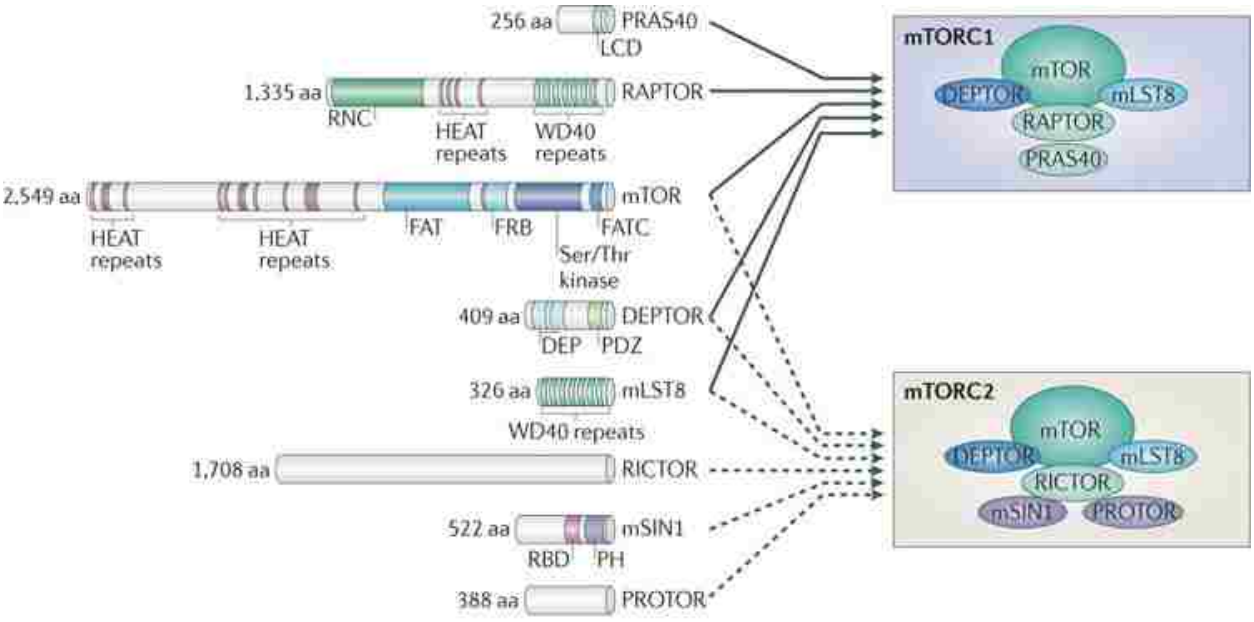

Figure 1.1 The composition of mTORC1 and mTORC2 mTORC1 consists of mTOR, mLST8, Raptor, PRAS40, and DEPTOR. Raptor and PRAS40 are unique to mTORC1, while mLST8 and DEPTOR are found in both mTORC1 and mTORC2. The domains of mTOR include N-terminal HEAT repeats, that comprise a large part of the mTOR and also enable protein-protein interaction, followed by a FAT domain and an FRB domain that constitutes the binding site for Rapamycin-FKBP12. The Ser/Thr kinase domain is next, with a small FATC domain at the C-terminal end. Raptor contains N-terminal conserved domains (RNC), followed by HEAT repeats in the center and a small WD-40 repeat domain at the C-terminus. Deptor contains DEP (Dishevelled, EGL-10 and pleckstrin) domains and PDZ (postsynaptic density of 95 kDa, Discs large and zonula occludens 1) domain. mLST8 consists entirely of seven WD-40 repeats that form a β-propeller structure. mTORC2 consists of mTOR, mLST8, Rictor, mSIN1, DEPTOR, and PROTOR. Rictor is an mTORC2-specific component that is structurally similar to Raptor. However, the domains of Rictor were not defined until very recently. mSIN1 is another mTORC2 specific component that contains RBD (Ras-binding domain) and PH (Pleckstrin homology) domains. PROTOR (Protein observed with Rictor) is also another accessory protein unique to mTORC2. Figure Reference [9].

1.2.3 mTOR kinase

mTOR is a 290 kDa kinase that belongs to the PIKK (phosphatidylinositol kinase-related kinase) family. The PIKK group consists of large molecular weight serine-threonine kinases including five members in addition to mTOR – ATM, ATR, DNA-PKcs, TRAP, and SMG1 [10, 11]. mTOR possesses the characteristic features of the PIKK family that include N-

terminal HEAT repeats (Huntingtin, ATM, eF3a, TOR) and a FAT (FAT, ATM, TRRAP) domain, followed by a PI3K-like catalytic domain, and a small FATC domain at the C-terminus [11]. The kinase domain of mTOR has the typical PI3K fold with an N-lobe and C-lobe. Additionally, mTOR kinase possesses some unique structural features such as an FRB domain in the N-lobe that binds to Rapamycin-FKBP-12 and an LBE (LST8 binding element) in the C-lobe that serves as a binding site for mLST8. (Figure 1.2)

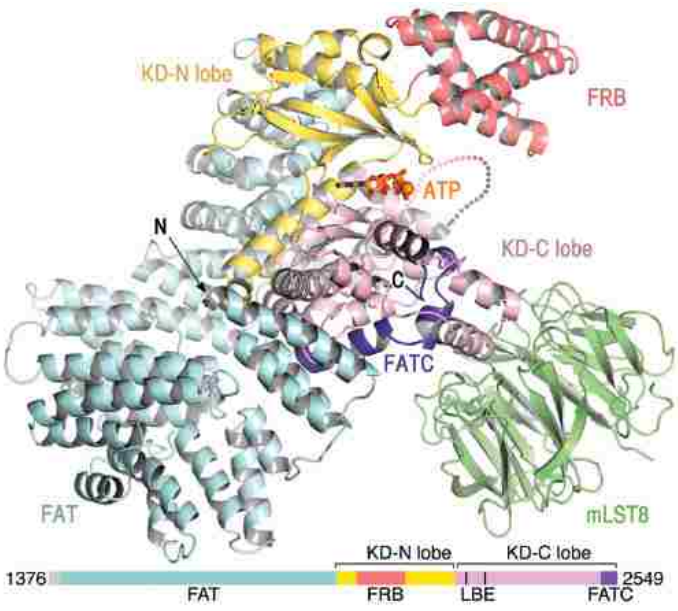

Figure 1.2 The structure of mTOR kinase The mTOR substrate binding cleft is sandwiched between the N-lobe (Yellow) and C-lobe (Purple) of the kinase domain. FRB (Pink) is an mTOR-specific domain that extends from the N-lobe to restrict the access to the substrate binding site. mLST8 (Green) interacts with FATC (Blue) domain and LBE (LST8 binding element) of the C-lobe and extends from the opposite side of FRB, further restricting the substrate binding groove. Figure reference [11].

The substrate binding site of mTOR resides in a 37 Å deep cleft flanked by the N-lobe and FRB domains on one side and the C-lobe-mLST8 structure on the other side [11]. The FRB domain and mLST8 together control the access to the substrate binding cleft of mTOR by

forming a narrow 8 Å opening. Binding of Rapamycin-FKBP-12 to the FRB domain further reduces the access to active site, thus inhibiting mTOR activity. The FRB domain also facilitates binding of an important substrate S6K1 to the active site. The FAT domain consists of three tetratricopeptide repeats (TRD), followed by C-terminal HEAT repeats. The FAT domain interacts with the kinase domain through highly conserved residues of TRD1 and the HEAT repeats, giving structural stability to mTOR.

1.2.4 mLST8

mLST8 is a 36 kDa protein with seven WD-40 repeats forming a β–propeller structure. mLST8 is also called Gβ–like due to its structural similarity with Gβ, a subunit of the G-protein heterotrimer. mLST8 is a positive regulator of mTOR kinase activity. The β-propeller blades of mLST8 stabilize the C-lobe of the mTOR kinase domain by interacting with its FATC and LBE loops [11]. mLST8-mTOR interactions comprise a crucial part of the mTOR substrate binding cleft that controls access to the active site. mLST8 deficient mouse embryonic fibroblasts showed decreased mTORC2 activity but have no change in mTORC1 activity, indicating that mLST8 is essential for mTORC2 signaling but may be dispensable for mTORC1 signaling [12]. mLST8 is an oncogene that enhances mTOR-mediated tumorigenesis. Several colon and prostate tumor cells showed higher expression of mLST8 compared to normal cells [13]. While mLST8 was not absolutely required for growth of normal cells, it promoted invasion of human colon cancer cells by controlling mTORC1 and mTORC2 activity. Thus, functions of mLST8 in mTOR signaling could be cell type specific. In the next chapter, we will describe our findings about the role of CCT in mLST8 expression and its assembly into mTORC1 and mTORC2. Due to oncogenic functions of mLST8, a thorough understanding of these processes can be used to

design small molecules to regulate the assembly of mLST8 into mTOR complexes, thereby modulating mTOR signaling.

1.2.5 mTORC1 components and structure

mTORC1 is symmetrical dimeric complex with a hollow rhomboid shape, containing two copies of mTOR, mLST8, and Raptor (Figure 1.3). The central core of the complex has the mTOR dimer formed by inter-molecular interactions between N-HEAT and M-HEAT domains of two mTOR molecules. mLST8 molecules are at the diagonally opposite ends, interacting with the C-lobe of the mTOR kinase domains. Raptor molecules are placed at the opposite ends of the longer axis, with their RNC domains interacting with HEAT domains of mTOR [14].

Raptor is a 150 kDa protein component of the mTORC1 core complex. Raptor comprises of three domains, namely RNC (Raptor N-terminal conserved) domains, HEAT repeats and a C-terminal WD40 repeat domain. Raptor facilitates nutrient sensing, cell size regulation, protein translation and autophagy by interacting with mTORC1 substrates like S6K1, 4EBP1, IRS-1 and ULK1. Raptor interacts with S6K1 and 4EBP1 through their TOS (TOR signaling) motifs. This interaction is critical for their activation, as indicated by severely impaired phosphorylation of TOS motif mutants [15]. Similarly, the interaction of Raptor with the SAIN (Shc and IRS-1 NPXY binding) domain of IRS-1 is required for its phosphorylation at Ser 636/639 [16].

The additional mTORC1 subunits, PRAS40 and DEPTOR, are nutrient-sensitive negative regulators of mTORC1. In nutrient deprived cells, PRAS40 and DEPTOR inhibit mTORC1 activity by binding to Raptor and mTOR respectively [17,18]. Under nutrient-rich conditions, PRAS40 and DEPTOR are phosphorylated at multiple sites by mTORC1, while DEPTOR is also phosphorylated at Thr 246 by AKT. This results in their dissociation from mTORC1, relieving the inhibitory effect [18, 19]

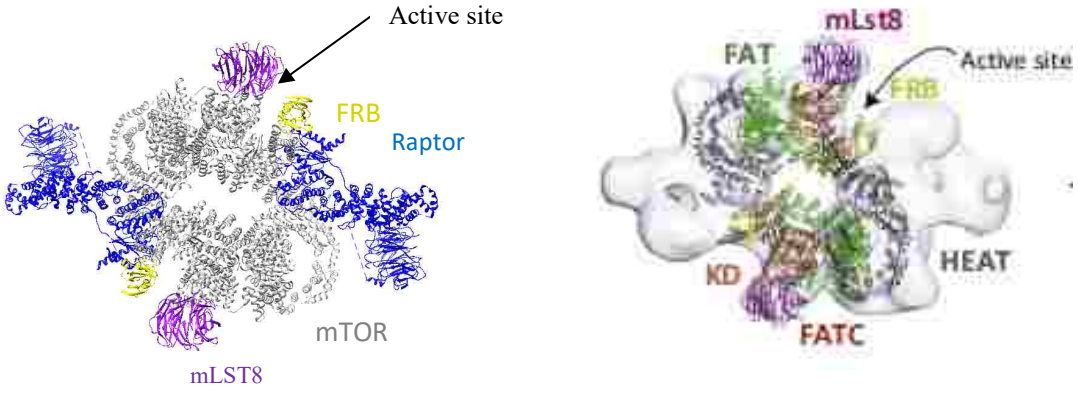

Figure 1.3 Structural comparison between mTORC1 and mTORC2 . mTORC1 structure is a hollow rhomboid shape with mTOR dimer in the center and mLST8/Raptor placed diagonally opposite to each-other. mLST8 and FRB domain of mTOR restrict the access to the active site. Super-imposition of mTOR-mLST8 crystal structure on mTORC2 EM density shows a similar arrangement of mTOR-mLST8 dimer as that of mTORC1. Figure references [14, 20].

1.2.6 mTORC2 components and structure

A high-resolution structure of mTORC2 is not yet available. Superimposition of the mTOR-mLST8 atomic model on an mTORC2 electron microscopy reconstruction reveals that mTORC2 has a similar arrangement of the mTOR-mLST8 dimer like mTORC1 [20]. Both Rictor and mSIN1 are required for an intact mTORC2 assembly, as their depletion caused dissociation of mTORC2 [21]. Being similar to Raptor, Rictor also contains N-terminal HEAT repeats and C-terminal WD-40 repeats [22]. Moreover, Rictor is predicted to have a ribosome binding site and a PH domain in the center. The C-terminus of Rictor shields the FKBP-Rapamycin binding site of mTOR, rendering mTORC2 insensitive to Rapamycin [20]. mSIN1 consists of an N-terminal domain, that interacts with mTORC2 components, a CRIM domain that is involved in substrate recruitment, and a C-terminal PH domain required for membrane attachment through phosphatidyl inositols [23]. While DEPTOR is an inhibitor of mTORC1

signaling, it activates mTORC2 signaling by abating the negative feedback inhibition of mTORC1 [19].

1.2.7 mTORC1 signaling

mTORC1 signaling is activated by a variety of ligands such as insulin, growth factors, amino acids, redox-potential, Wnt signaling, and cytokines [17]. In a canonical mTORC1 pathway, binding of insulin to the insulin receptor triggers the conversion of phosphatidylinositol 4,5–bisphosphate (PIP2) to phosphatidylinositol 3,4,5- trisphosphate (PIP3). PIP3 then recruits AKT to the plasma membrane by interacting with its pleckstrin homology (PH) domain (Figure 1.4). AKT is fully activated by two phosphorylation events: i) phosphorylation at Thr308 by 3- phosphoinositide dependent protein kinase 1 (PDK1), which also adheres to the membrane by a PH domain, and ii) phosphorylation at Ser473 by mTORC2. Downstream of AKT, is a tuberous sclerosis complex (TSC) that consists of TSC1 and TSC2. The TSC1/2 dimer is a negative regulator of mTORC1 [24]. TSC exerts its inhibitory effect by facilitating hydrolysis of Rheb-GTP, an activator of mTORC1 [25]. Rheb is a lysosomal protein that recruits mTORC1 to the surface of lysosomes and also enables its activation. AKT phosphorylates TSC2, causing its dissociation from the TSC complex and disrupting its ability to hydrolyse Rheb-GTP [25]. Accumulated Rheb-GTP then stimulates mTORC1. Alternatively, TSC can be inhibited by MAPK/ERK pathway, Wnt signaling, and TNFα, ultimately resulting in mTORC1 activation [17,26,27]. Cellular stress conditions like hypoxia or DNA damage activate TSC through REDD1 and AMPK respectively, thereby curbing the mTORC1 activity [28,17]. Thus, numerous pathways converge at TSC to modulate mTORC1 signaling (Figure 1.4).

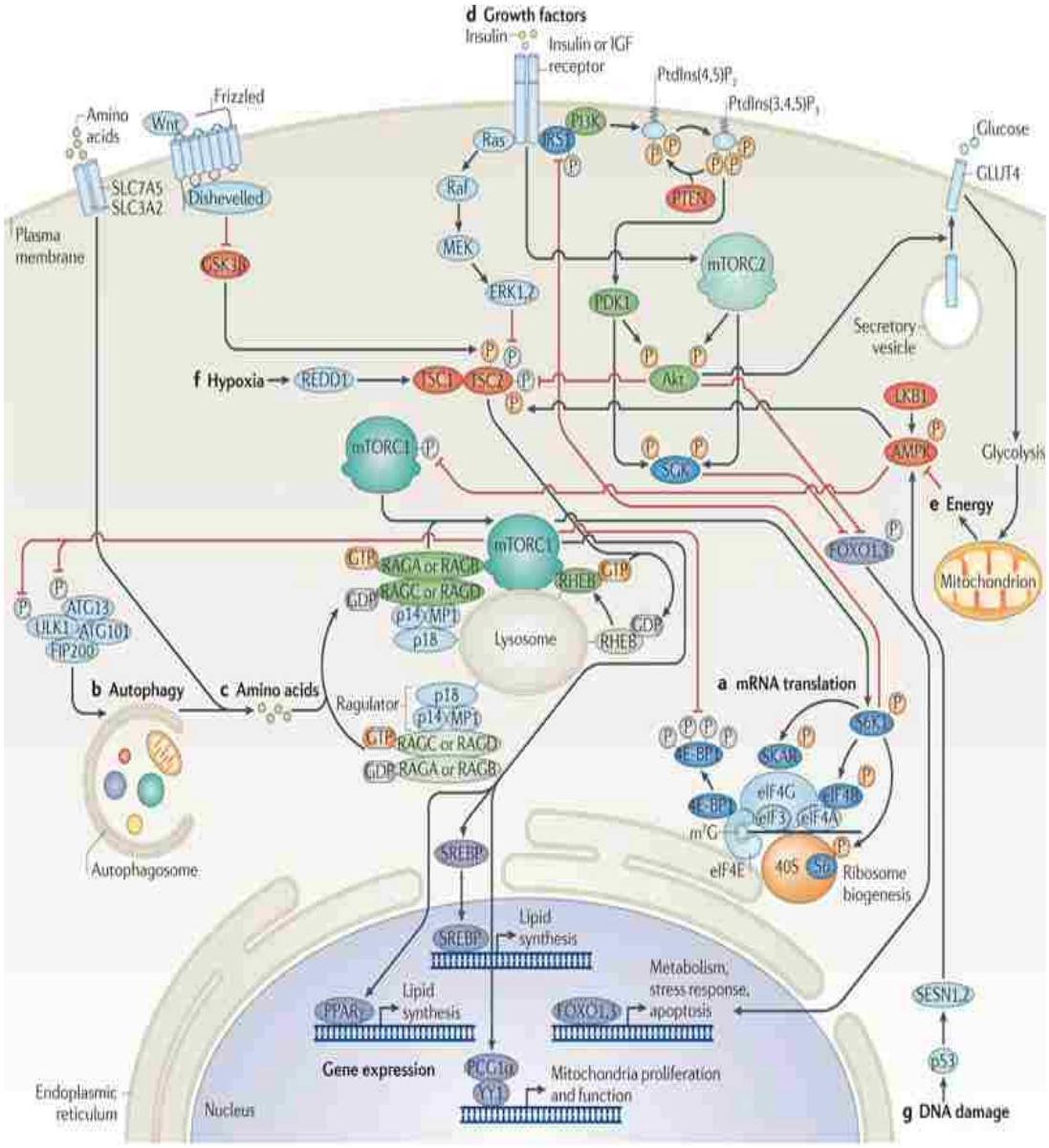

Figure 1.4 The overview of mTORC1 and mTORC2 signaling. mTORC1 is activated when insulin binds to the insulin receptor, followed by membrane attachment and phosphorylation of AKT at Thr308 by PDK1 and at Ser473 by mTORC2. AKT activates mTORC1 by relieving the inhibitory effect of TSC. Alternatively, Wnt signaling (GSK3β), AMPK, and hypoxia (REDD1) also activate mTORC1 by inhibiting TSC. Amino acids activate mTORC1 through RAG GTPases which deliver mTORC1 to lysosomes. mTORC1 phosphorylation promotes translation by activating S6K1 and inhibiting 4EBP1 and also inhibiting autophagy by suppressing ULK1. mTORC2 signaling is initiated by insulin-mediated activation of insulin receptor or insulin-like growth factor receptor, that eventually leads to activation of the survival kinase, AKT. Fully activated AKT exerts its oncogenic effect by inhibiting the tumor suppressor FOXO. mTORC1 signaling generates a negative feedback inhibition loop for mTORC2 through phosphorylation-dependent degradation of IRS1. PTEN is another negative regulator of mTORC2, which restricts membrane attachment of mTORC2 by dephosphorylating PIP3. Figure reference [30].

A second way to activate mTORC1 is through amino acids. Amino acids directly stimulate mTORC1 by its Rag-GTPases mediated delivery to lysosomes, where it meets Rheb-GTP for its activation [29]. Upon activation, mTORC1 phosphorylates 4EBP1 at Thr36 and 45 and S6K1 at Thr389 [17]. Under poor nutrient conditions, 4EBP1 represses translation by binding to eIF4e and preventing its entry into the translation initiation complex. Under nutrient-rich conditions, 4EBP1 is phosphorylated by mTORC1, releasing eIF4e which then enters the initiation complex [31]. The complete initiation complex containing 40S ribosomal subunit, eIF4e and several other transcription factors like eIF4A, eIF4G, eIF4B induces 5′-cap dependent translation. Phosphorylated S6K1 also enhances translation by phosphorylating ribosomal protein S6, which increases translation rates and by phosphorylating and triggering the degradation of PDCD4, an inhibitor of eIF4B [Figure 1.4 and 17].

1.2.8 mTORC2 signaling

Primarily, mTORC2 signaling is initiated by insulin binding to its receptor and activating PI3K (phosphatidylinositol 3-kinase) which then phosphorylates PIP2 to PIP3. PIP3 facilitates recruitment of mTORC2 to the plasma membrane, which binds PIP3 via the PH domain of mSIN1 [Figure 1.4]. Before its attachment to the plasma membrane, the PH domain of mSIN1 hinders the substrate binding site of mTOR. However, in a membrane-bound state the PH domain is rearranged to remove the steric hindrance, thereby activating mTORC2. Functional mTORC2 then phosphorylates and activates AKT which promotes cell survival by inhibiting the tumor suppressing transcription factor, FoxO3a [32]. Moreover, mTORC2 also activates several members of the AGC kinase family: PKC-α, γ, ε, δ, and ζ that are involved in cytoskeletal remodeling, and SGK1 which regulates ion transport [17].

mTORC2 is negatively regulated by PTEN (phosphatase and tensin homolog) and mTORC1(Figure 1.4). PTEN is a lipid phosphatase that dephosphorylates PIP3 to PIP2, thus limiting membrane recruitment of mTORC2. Insulin activation of mTORC1 initiates a feedback inhibition loop in which mTORC1 activation of S6K1 leads to phosphorylation and degradation of IRS1 (insulin receptor substrate-1). mTORC1 also phosphorylates an adaptor protein called GRB10 (Growth factor receptor-bound protein 10) that inhibits mTORC2 signaling by binding to insulin receptor or IGF (Insulin-like growth factor receptor). GRB10 is especially found in the cells lacking TSC mediated inhibition of mTORC1 [33].

1.2.9 Chaperones in mTORC assembly

Molecular chaperones maintain cellular homeostasis by folding a variety of proteins and enabling their assembly into functional multi-protein complexes. Discrepancies in protein folding lead to deposition of unstructured protein aggregates, causing several neurodegenerative and age-related disorders like Parkinson's disease, Alzheimer's disease, and Type-II diabetes. The chaperone network in a cell comprises of heat shock proteins (HSP) 70 and 90 and chaperonins. Members of PIKK family, including mTOR, are folded by supramolecular protein machinery, consisting of Hsp90 as a chaperone and TTT/R2TP complex as a co-chaperone [34]. The TTT protein complex consists of Tel2, Tti-1, and Tti-2 (Tel2 interacting components 1, and 2). Tel2 interacts with the nascent mTOR polypeptide in an HSP-90 dependent manner. Depletion of Tel2 in mouse embryonic fibroblasts severely reduced the assembly of newly synthesized mTOR into mTORC1/2, indicating its importance for the integrity mTOR complexes [35]. The R2TP complex (Rvb1, Rvb2, Tah1, and Pih1) acts as a functional bridge that connects Hsp90 and the TTT complexes. Additionally, mTORC1 requires an energy-sensing adaptor molecule, called WAC (WW domain containing adaptor with coiled-coil) which assembles TTT

and R2TP complexes under nutrient-rich conditions [36]. Although folding of mTOR by Hsp90 and its co-chaperones has been extensively studied, little is known about the folding and assembly of other mTORC components.

1.2.10 CCT as a possible chaperone for mLST8 and Raptor

CCT (cytosolic chaperonin containing tailless complex polypeptide-1) is a member of group II chaperonin family. Chaperonins are cytosolic proteins with a multimeric double-ringed structure that provides a central isolated cavity for protein folding (Figure 1.5). Group I chaperonins involve bacterial GroEL/GroES systems, while Group II chaperonins involve thermosomes in archaea and CCT in eukaryotes [37]. CCT (also known as TriC) is a 1M-Da barrel-shaped complex with two identical rings, stacked on top of each-other. Each ring consists of 8 structurally homologous subunits (CCT1-8), arranged as shown in the (Figure 1.5A). CCT subunits are highly conserved and also share about 30% sequence identity with each other. Each CCT subunit consists of 3 domains – apical, intermediate, and equatorial (Figure 1.5B). The apical domains are exposed to the cytosol and are involved in substrate binding. The equatorial domains are at the center of the structure and possess ATPase activity. The intermediate domains link ATP hydrolysis in the equatorial domains to conformational changes in the apical domains, enabling substrate encapsulation and folding [38].

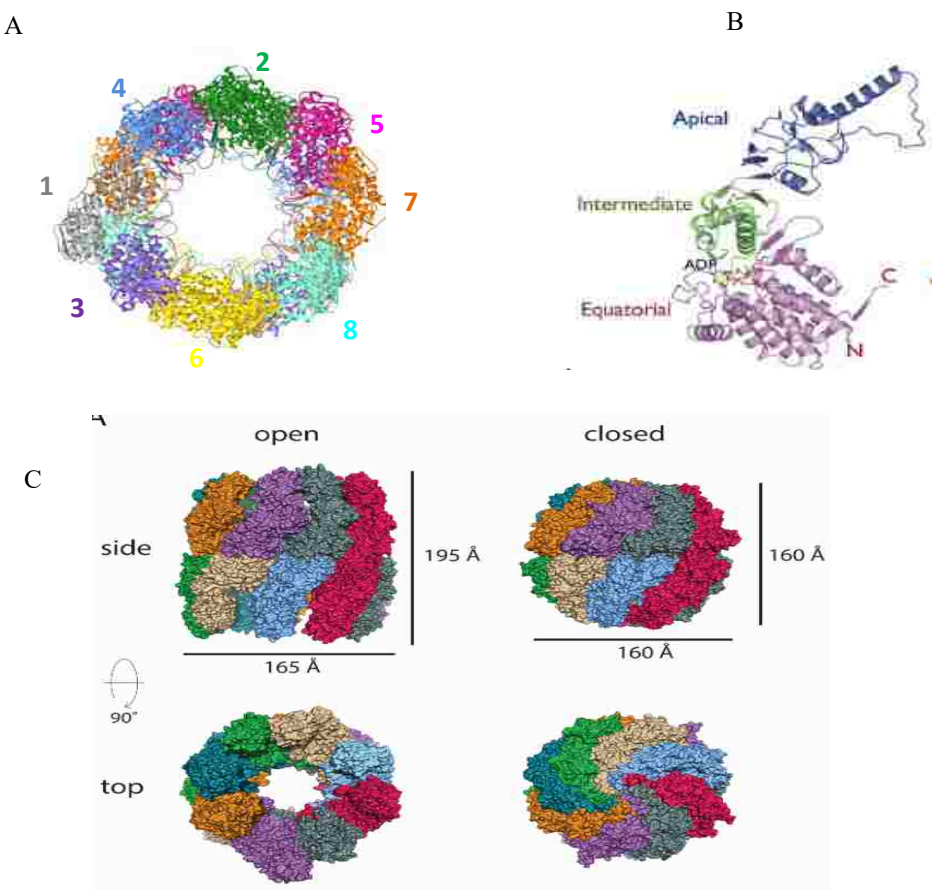

Figure 1.5 Architecture of CCT

A) The domain arrangement of CCT. CCT domains are arranged in a clockwise manner in the following order: 1 (alpha), 4 (delta), 2 (beta), 5 (epsilon), 7 (eta), 8 (theta), 6 (zeta), and 3 (gamma). B) Structural organization of individual domain of CCT. C) Open and closed conformations of CCT.

The CCT folding cycle consists of an open conformation in which the nucleotide binding site of the equatorial domains is either empty, or ADP-bound and the apical domains are accessible to the substrates [39]. Binding of ATP triggers a conformational change in apical domains that facilitates the closed conformation and substrate entrapment. Open and closed confirmation cycles can continue until the substrate reaches its native folding state. The completely folded substrate is released after ATP hydrolysis and sometimes also requires the presence of a co-chaperone.

CCT folds about 10-15% of eukaryotic proteome which involves some important protein substrates like actin, tubulin, VHL (von Hippel-Lindau tumor repressor), p53, CDC20, and Gβ [40–43]. CCT substrates have a variety of complex structural folds, one of which is WD-40 repeats that are folded into β-propeller domains. In Chapter 2, we investigate the role of CCT in mTORC assembly since mLST8, Raptor and Rictor are known to possess WD-40 repeats. A study in yeast showed that over-expression of CCTζ repressed the abnormal phenotypes caused by LST8 and TOR mutations, indicating a possible role of CCT in mTORC assembly [44]. Structural similarities between mLST8 and Gβ pointed towards the possibility of mLST8 binding to CCT, which was in fact confirmed in an autophagy interactome study [45]. Moreover, another study showed that S6K1 phosphorylates CCTβ subunit at Ser260, thus possibly regulating the function of CCT [46]. These facts encouraged us to investigate the role of CCT in mTORC assembly.

1.2.11 PhLP1 as a co-chaperone for CCT.

PhLP1 (Phosducin-like protein 1) is a member of the highly conserved phosducin gene family. PhLP1 is an indispensable co-chaperone for CCT-mediated Gβ folding and Gβγ assembly. Depletion of PhLP1 severely affects G-protein signaling due to an inability to form Gβγ dimers [47]. Rod and cone photoreceptor cell-specific PhLP1 knockout mice had radically diminished photopic and scotopic visual responses due to disruption of G-protein signaling in the retina [48, 49]. Structural studies of Gβ-CCT and PhLP1-Gβ-CCT ternary complex revealed that PhLP1 is required for stabilization of the Gβ structural fold and release of Gβ from the folding cavity [50].

In our study, we have explored the possibility of PhLP1 as a co-chaperone for mLST8-CCT interaction. We also report evidence indicating a novel role of PhLP1 in the degradation of Raptor.

1.3 **Conclusion**

WD40 repeats are the characteristic substrate folds recognized by the cytosolic chaperonin CCT. We hypothesized that CCT and its co-chaperone PhLP1 could be involved in the assembly of mTOR complexes since mLST8, Raptor and Rictor are known to contain WD-40 repeats. Moreover, mLST8 is structurally very similar to Gβ, a known substrate of CCT/PhLP1, and the reported interaction between CCT and mLST8 further encouraged us to pursue the hypothesis. The next chapter describes several biochemical and structural studies that we performed to fully investigate the role of CCT and PhLP1 in folding and assembly of mLST8 into mTOR complexes. These studies have also identified Raptor as a new substrate for CCT. We have obtained the high-resolution cryo-EM structure of the mLST8-CCT complex and performed signaling and assembly experiments that indicate the involvement of CCT and PhLP1 in mTOR signaling. The high-resolution cryo-EM structure of mLST8-CCT, combined with mass spectrometric cross-linking data will provide a detailed mechanism of mLST8 folding. These studies can be pharmacologically important because the CCT interaction site of mLST8 or Raptor could be targeted by small molecules, thus interfering with the formation of intact mTOR complexes.

CHAPTER 2 : ROLE OF CCT AND PhLP1 IN FOLDING AND ASSEMBLY OF THE mTOR COMPLEXES

2.1 Summary

mTOR kinase regulates cellular growth and metabolism through two distinct complexes, called mTORC1 and mTORC2. In this chapter, we have described biochemical and structural experiments performed to investigate the role of the cytosolic chaperonin CCT and its co-chaperone PhLP1 in the assembly of the mTOR complexes. We have discovered that CCT contributes to mTORC1 and mTORC2 assembly by folding mLST8, a component common to both of them. We have also identified Raptor as a novel substrate of CCT and established that CCT also contributes to the mTORC1 assembly by folding Raptor. We have shown that the co-chaperone PhLP1 behaves differently in the case of mLST8 and Raptor. While PhLP1 is required for folding of mLST8, it facilitates degradation of Raptor. We have also obtained the high-resolution cryo-EM structure of the mLST8-CCT complex, coupled with mass spectrometric cross-linking. The structural comparison between mLST8-CCT and Gβ-CCT indicates that mLST8 is positioned quite differently in the CCT folding cavity compared to Gβ. While Gβ sits near the opening of the substrate cavity, mLST8 is buried deep inside it. Thus, the mechanism of folding for Gβ and mLST8 is distinct, despite their structural similarity.

2.2 Introduction

mTOR responds to a plethora of extracellular and intracellular signals to stimulate cell division, protein and lipid synthesis, and cytoskeletal reorganization. There are two mTOR signaling complexes, namely mTORC1 which contains mTOR, mLST8, and Raptor, and mTORC2 which comprises of mTOR, mLST8, Rictor, and mSIN1. The unique components of

mTOR complexes impart different properties to mTORC1 and mTORC2, and hence they differ in terms of upstream regulators and downstream effectors, cellular functions, sub-cellular localization, and rapamycin sensitivity. Various negative regulators like DEPTOR, PRAS40, TSC, GRB10, and PTEN act at various stages of the mTOR signaling cascade to prevent its uncontrolled activation. Faulty control mechanisms of the mTOR pathway yield intrinsically active mTOR, eventually causing various hyperimmune disorders, malignancies, and Type-II diabetes.

Protein folding is essential to maintain cellular homeostasis. Misregulations in protein folding are implicated in various neurodegenerative disorders and aging. Components of mTOR complexes have intricate structural folds that require assisted folding. mTOR kinase is a large multi-domain protein that is folded by a supramolecular folding machinery consisting of HSP90, TTT (Tel2, Tti-1, and Tti-2), and R2TP (Rvb1, Rvb2, Tah1, and Pih1). However, it is not clear how other mTOR components are folded and assembled into mTOR complexes. Our study sheds light on the folding mechanisms for mLST8 and Raptor by the cytosolic chaperonin CCT and its co-chaperone PhLP1. We reasoned that mLST8 might be folded by CCT due to its structural resemblance to Gβ, an established substrate of CCT. Both mLST8 and Gβ have the conserved WD-40 repeat domains that are assembled into β-propeller structures. We also tested the possibility of Raptor and Rictor binding to CCT, since both of them possess WD-40 repeats. We have measured the effects of CCT/PhLP1 knockdowns on the mTORC assembly and signaling. Our data shows that loss of CCT affects the expression levels of mLST8 and Raptor, thereby affecting the mTORC assembly and signaling. We have also obtained a molecular view of the interaction between mLST8 and CCT through cryo-EM and mass-spectrometric cross-linking

structural analysis. These studies provide a wealth of information about the involvement of CCT and PhLP1 in the mTORC assembly that could be used to design small molecules that control the mTOR signal by affecting the formation of mTOR complexes.

2.3 Methods

2.3.1 Purification of the mLST8-CCT, PhLP1-mLST8-CCT, and Raptor-CCT complex

For purifications, the respective constructs were transfected in human embryonic kidney (HEK)-293T cells grown in 1:1 DMEM F-12 media with 10 % fetal bovine serum (FBS). Cells were cultured in T-175 flasks and were transfected at 80 % confluency with polyethyleneimine (PEI). A total of 90 μg of the plasmid DNA were transfected with 3 μg per microliter of PEI. For the purification of mLST8-CCT, HEK-293T cells were co-transfected with a pcDNA3.1 vector containing human PhLP1 with a c-Myc-His_6 tag at the C-terminus and the same vector containing human mLST8 with a double Strep-Flag tag at the N-terminus and an HPC4 tag at the C-terminus. For Raptor over-expression, HEK-293T cells were transfected with a pDEST40 vector containing human Raptor with an HPC4-Strep-His_6 tag at the N-terminus.

In the purification of the mLST8-CCT and PhLP1-mLST8-CCT complexes, the cell lysate was first applied to a HisPur (Thermo Fisher Scientific) packed column equilibrated with cobalt equilibration buffer (20 mM HEPES pH 7.5, 20 mM NaCl) and circulated at 4 ºC for one hour. The column was washed with five column volumes of cobalt wash buffer (20 mM HEPES pH 7.5, 20 mM NaCl, and 0.05 % CHAPS) and eluted with 2.5 column volumes of cobalt elution buffer (20 mM HEPES pH 7.5, 20 mM NaCl, 250 mM imidazole, and 0.05 % CHAPS). For the PhLP1-mLST8-CCT complex, the HisPur column eluate was loaded onto a Strep-Tactin column

equilibrated with Strep equilibration buffer (20 mM HEPES pH 7.5, 20 mM NaCl, and 2 mM $CaCl_2$), washed with three column volumes of Strep wash buffer (20 mM HEPES pH 7.5, 20 mM NaCl, 2 mM $CaCl_2$, and 0.05 % CHAPS), and eluted with five column volumes of Strep elution buffer (20 mM HEPES pH 7.5, 20 mM NaCl, 2 mM $CaCl_2$, 2.5 mM desthiobiotin, and 0.05 % CHAPS). For the mLST8-CCT complex purification, after loading the Strep column was washed with three column volumes of high salt wash buffer and one column volume of Strep wash buffer and eluted with five column volumes of Strep elution buffer. The purpose of the high salt wash buffer was to remove PhLP1 from mLST8-CCT complex by disrupting electrostatic interactions with high ionic strength.

An HPC4 column (Roche) was used for the purification of Raptor-CCT complex. The lysate from cells over-expressing HPC4-tagged Raptor was loaded on to the HPC4 resin, and the column was washed twice with two column volumes of high salt wash buffer and once with two column volumes of Strep wash buffer. Raptor was eluted in five elution steps, each with one column volume of HPC4 elution buffer according to the manufacturer's protocol.

The protein complexes were concentrated to ~ 2 mg/mL by centrifugation with a 30 kDa molecular weight cutoff filter (Millipore). The purity of the samples was confirmed by SDS-PAGE and immunoblotting. The concentrated samples were flash frozen in liquid nitrogen and stored at -80 ^{o}C until use. Purified mLST8-CCT complexes were further analyzed by cryo-EM and XL-MS.

2.3.2 Cryo-EM

Purified mLST8-CCT and PhLP1-mLST8-CCT complexes were applied to glow discharged Quantifoil 1.2-µm holey carbon grids, blotted, and fast-frozen in liquid ethane. Low-

dose images (<10 $e^-/Å^2$) of the complexes were taken on a Talos Artica 200 kV transmission electron microscope. Image classification was done with the reference-free method, and the selected averages were obtained to generate a reference volume using common lines, which was subsequently applied to the 3D reconstruction procedure. Chimera was used to visualize and dock the atomic structure.

2.3.3 Crosslinking coupled with mass spectrometry

About 200 μg of the protein complexes was taken to be crosslinked in 25 mM HEPES pH 8.0, 100 mM KCl, and 325 μM of a 50 % mixture of H12/D12 disuccinimidyl suberate (DSS) or H6/D6 disuccinimidyl glutarate (DSG) (Creative Molecules) at 37 ºC for half an hour. The reaction was quenched by adding 50 mM ammonium bicarbonate to the crosslinked sample and incubating at 37 ºC for 15 minutes. The sample was dried by a vacuum concentrator, denatured in 100 mM Tris-HCl pH 8.5 and 8 M urea, reduced with 5 mM TCEP at 37 ºC for 30 minutes, and alkylated with 10 mM iodoacetamide at room temperature in the dark for 30 minutes. The sample was diluted with 150 mM ammonium bicarbonate to bring the urea concentration to 4 M, and proteins were digested with 4 μg of lysyl endopeptidase (1:50 enzyme: substrate ratio) at 37 ºC for two hours. Subsequently, urea was diluted to 1 M, and proteins were further digested with trypsin at a 1:50 ratio at 37 ºC overnight. Peptide fragments were purified on a C18 column (Waters), dried, and reconstituted in 35 μL size exclusion column (SEC) mobile phase (70:30:0.1 water: acetonitrile: TFA). Crosslinked peptide fragments were enriched by SEC using a Superdex Peptide PC 3.2/30 column on an AKTA pure system (GE Healthcare) at a flow rate of 50 μL/min. The fractions with the highest peptide concentration were dried and resuspended in 2 % formic acid.

2.3.4 Mass spectrometry

The enriched crosslinked peptide samples were separated using a Thermo Fisher Scientific EASY-nLC 1000 Liquid Chromatograph system with a 15 cm Picofrit column (New Objective) packed with Reprosil-Pur C18-AQ of 3 um particle size, 120 Å pore size and gradient of 5-95 % acetonitrile in 5 % DMSO and 0.1 % formic acid over 185 minutes and at a flow rate of 350 uL/min. The column was coupled via electrospray to an Orbitrap Velos Pro mass spectrometer. The resolution of MS1 was 30,000 over a scan range of 380-2000 m/z. Peptides with a charge state 3+ and greater were selected for HCD fragmentation at a normalized collision energy of 35 % with 3 steps of 10 % (stepped NEC) and a resolution of 7,500. Dynamic exclusion was enabled with a 10 ppm mass window and a one-minute time frame. Samples were run in duplicate.

2.3.5 XL-MS analysis

The xQuest/xProphet peptide search engine was used to identify crosslinked peptides and specific lysine residues and to evaluate the quality of each hit from the mass spectrometry data set. Tandem mass spectra for parent ions with a mass shift of 12.075321 Da for DSS crosslinker and 6.04368 Da for DSG crosslinker and a charge of +2 to +7 were classified as isotopic pairs and evaluated in ion-tag mode with the following parameters: 2 missed cleavages, 5-50 amino acid peptide length, carbamidomethyl fixed modification (57.02146 Da mass shift), oxidation variable modification (15.99491 Da mass shift), 138.0680796 Da mass shift for intra- and inter-protein crosslinks, 156.786442 and 155.0964278 Da mass shifts for mono-links, MS1 tolerance of 10 ppm, and MS2 tolerance of 0.2 Da for common ions and 0.3 Da for crosslink ions.

The peptide sequence database was created by xQuest based on the amino acid sequence of human mLST8 and CCT. Crosslink hits were screened with the following criteria: <10 % false discovery rate, <10 % total ion counts, -4 to 7 ppm MS1 tolerance window, >20 xQuest Id-Score, and >4 fragmentation events per peptide.

2.3.6 siRNA knockdowns and transfections in HEK 293T cells

Negative control, CCT, and PhLP1 siRNA were purchased from Dharmacon. Knockdowns were performed with Lipofectamine 2000/3000 at 30-40% confluency. Cells were replenished with new media 3-4 hours after the knockdown. Cells were transfected with the components of mTORC1 or mTORC2 between 24-30 hours after knockdown at 90% confluency. The cells were fed again with fresh media 3 hours after transfection. Media was also replaced 48 hours after transfection. Cells were harvested 96 hours after knockdown for immunoprecipitations and immunoblotting.

2.3.7 CRISPR knockouts and transfections in HEK 293T cells

sgRNA primers targeting the 5′-end near the coding region of CCTε were designed and ordered from Integrated DNA Technologies. The primers were PCR amplified and cloned into the CRISPR plasmid pX459 (Addgene). PX459 has a U6 promoter that generates guide RNA containing the target sequence for CCTε followed by the Cas9 handle. PX459 also has the sequences encoding Cas9 DNase and puromycin resistance. The sgRNA binds to its complementary DNA through its target sequence and also binds to the Cas9 DNase through the Cas9 handle. The target gene is knocked out as the Cas9 makes double-stranded DNA breaks at the target sequence which are then repaired by a non-homologous end joining repair mechanism, resulting in insertions or deletions. HEK 293T cells were transfected with CRISPR plasmids

containing CCTε sgRNA or a control plasmid without the sgRNA sequence at 25-40% confluency with Lipofectamine 2000. The cells were fed with fresh media 3 hours after transfection. The cells were then transfected with the components of mTORC1 or mTORC2 48 hours after the transfection of CRISPR plasmids, followed by feeding with new media containing 10 μg/mL puromycin after 3 hours. The puromycin concentration was maintained until harvest by replacing the media with new puromycin containing media every 24-48 hours. The cells were harvested at 120 hours after knockdown for immunoprecipitations and immunoblotting.

2.3.8 Ubiquitin assay

After treating HEK-293T cells with siRNA targeting PhLP1, the cells were co-transfected with a pcDNA3 vector containing human ubiquitin with an N-terminal HA tag (Addgene) and a pDEST40 vector containing human Raptor with an N-terminal Strep-tag using Lipofectamine 2000. Cells were fed with fresh media four hours post-transfection and treated with 10 μM of MG-132 (Ubiquitin-Proteasome Biotechnologies) two to four hours prior to harvest. At 48 hours post-transfection, cell lysates were prepared and immunoprecipitated with a α-HA tag antibody and immunoblotted.

2.3.9 Insulin signaling

HEPG2 cells were treated with 80 nM of siRNA targeting CCTα/ε, PhLP1, mLST8 or Raptor using Lipofectamine 3000 following the manufacturer's protocol for reverse transfection. On the third day after the siRNA transfection, cells were starved overnight with serum-free media. Subsequently, the cells were treated with 1 μM insulin for 30 minutes to activate mTORC1 or 50 nM insulin for 10 minutes to activate mTORC2. The effects on mTORC1 and mTORC2 signaling were analyzed by SDS-PAGE and immunoblotting the cell lysates for

phosphorylation at IRS1 S636/639 and AKT S473, respectively. Total CCT, PhLP1, mLST8, Raptor, AKT, and IRS1 were also immunoblotted to assess the respective knockdown and expression level.

2.3.10 shRNA knockdowns

The donor retroviral vectors containing shRNA for CCTβ or control shRNA targeting GFP were purchased from Sigma-Aldrich. The viruses were made by co-transfecting the donor vectors with packaging vector pCMV-dR8.1 and envelope vector pVSVG. Supernatants containing viruses were collected 48 hours after transfection. T75 flasks containing HEPG2 cells were transduced with GFP or CCT viruses with 4 μg/mL polybrene and media was replaced 4 hours after transduction. To select the successfully transduced cells, they were split 24 hours after transduction in media containing 5 μg/mL of puromycin. The cells were harvested 72 hours after splitting in HEPES buffer with 1% NP40 containing protease and phosphatase inhibitors. The cell lysates were run on SDS-PAGE gels and immunoblotted for the respective proteins as shown in the figures.

2.4 Results

2.4.1 mLST8, CCT, and PhLP1 form a ternary complex

In order to test for an interaction between CCT and mLST8, we transfected HEK 293T cells with either Flag-tagged mLST8 or empty vector. mLST8 was then immunoprecipitated (IPed) with a Flag antibody, and the presence of CCT as a co-immunoprecipitate (co-IP) was tested by immunoblotting. Compared to the empty vector control, we saw a strong co-IP of CCTε in the Flag-mLST8 IP, indicating that mLST8 and CCT interact with each other (**Figure 2.1 A**). We also verified the interaction between PhLP1 and mLST8 by co-transfecting HEK

293T cells with Flag-mLST8 and His_6-tagged PhLP1 constructs. We immunoprecipitated PhLP1 with a His_6 antibody and saw a strong band of Flag-mLST8 in the co-IP which was not seen in the empty vector control, indicating that mLST8 interacts with PhLP1 (**Figure 2.1B).**

Since Gβ forms a ternary complex with PhLP1 and CCT and mLST8 was found to interact with both of them, we wanted to know whether mLST8 also forms a ternary complex with CCT and PhLP1. To test this possibility, we depleted HEK 293T cells of CCT with siRNA and tested its effect on the interaction between mLST8 and PhLP1. We observed a 45% decrease in the mLST8 bound to PhLP1 with a 50% CCT knockdown, indicating that the mLST8-PhLP1 interaction is dependent on CCT and thus, all three proteins could be a part of the same complex (**Figure 2.1 C**).

We also performed a double IP experiment to confirm whether mLST8, CCT and PhLP1 form a ternary complex (**Figure 2.1D**). We co-transfected HEK 293T cells with PhLP1 containing a TEV protease recognition sequence followed by a c-Myc tag and mLST8 with a Flag-tag. In the first IP, we pulled down PhLP1 with Myc-antibody and found CCTε and Flag-mLST8 in co-IP. We then treated the IPs with TEV protease to remove all the PhLP1-bound complexes from the beads. In the second IP, we pulled down CCT with a CCTε antibody and again found PhLP1 and mLST8 in the co-IP. We also performed empty vector controls for both the IPs and did not see any co-IP bands indicating that the interactions we observed were specific. The presence of mLST8 in both the IPs indicates that it simultaneously interacts with PhLP1 and CCT, thus confirming the possibility of the ternary complex.

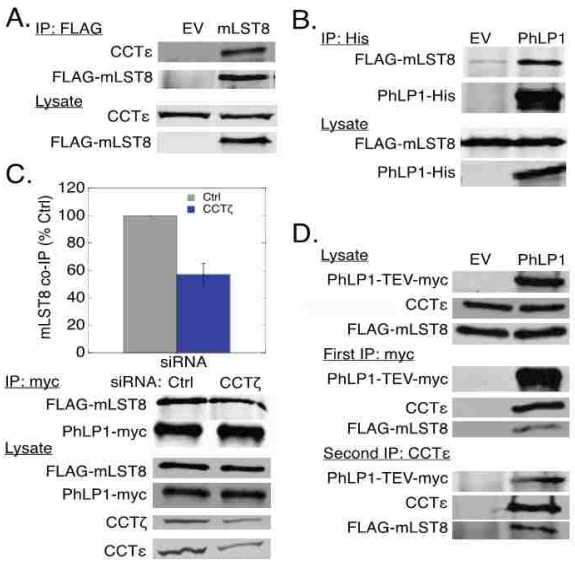

Figure 2.1 mLST8, CCT and, PhLP1 form a ternary complex. A) Interaction of mLST8 with CCT. HEK-293T cells were transfected with Flag-mLST8 or empty vector (EV). Lysates were immunoprecipitated with a Flag antibody and immunoblotted for CCTε and Flag-mLST8. B) Interaction of mLST8 with PhLP1. Cells were co-transfected with Flag-mLST8 and PhLP1-c-Myc-His or empty vector. Lysates were immunoprecipitated with a His_6 tag antibody and immunoblotted for Flag-mLST8 and PhLP-His. C) CCT depletion inhibited mLST8 interaction with PhLP1. Cells were treated with CCTζ or control siRNA, co-transfected with Flag-mLST8 and PhLP1-c-Myc-His and immunoprecipitated with a Myc-antibody. Immunoprecipitates and cell lysates were blotted as indicated. D) Double immunoprecipitation revealed PhLP1-mLST8-CCT ternary complex. Cells were co-transfected with Flag-mLST8 and PhLP1-TEV-c-Myc or empty vector and immunoprecipitated with a Myc antibody. Complexes were released from the beads by TEV cleavage and immunoprecipitated again with a CCTε antibody and immunoblotted as indicated.

2.4.2 C-terminal β-propeller domain of Raptor binds to CCT

Raptor is a 150 kDa multimeric protein with a C-terminal WD40-repeat domain. Therefore, we wanted to know whether Raptor also binds to CCT. We transfected HEK 293T cells with either empty vector or HA-tagged Raptor. We pulled down Raptor with an HA antibody, and looked for the presence of CCT in the co-immunoprecipitate (**Figure 2.2A**). Similarly, we immunoprecipitated CCT with a CCTε antibody and observed that the HA-Raptor is also pulled down with CCT (**Figure 2.2A**), thus indicating that CCT and Raptor interact with

each other. We wanted to know whether Raptor binds to CCT specifically through the C-terminal WD-40 repeat domain. Therefore, we made HA-tagged truncations of Raptor, such that the N-terminal Raptor construct (residues 1-1019) contained all the subdomains except the WD-40 repeats, whereas the C-terminal Raptor construct (residues 1020-1335) consisted entirely of the WD-40 repeats. We observed a strong interaction between the C-terminal Raptor construct and CCT (**Figure 2.1B**), whereas the N-terminal construct did not interact with CCT (**Figure 2.1C**), confirming our prediction that only the C-terminal β-propeller region of Raptor binds to CCT. The Raptor-CCT interaction was also observed to some extent in the purified Raptor-CCT complexes (**Figure 2.1D**). As indicated by Coomassie gel staining of the purified complex, the amount of CCT recovered in the final purification was in a sub-stoichiometric amount. This could be either due to transient intracellular interaction between Raptor and CCT or dissociation of Raptor during the process of purification.

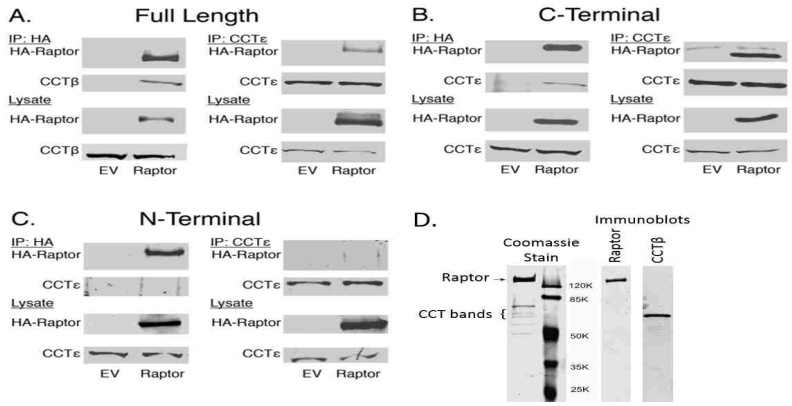

Figure 2.2 C-terminal β-propeller domain of Raptor binds to CCT. A) Full-length Raptor binds to CCT. HEK-293T cells were transfected with the HA-Raptor or empty vector. Lysates were immunoprecipitated with an HA antibody or a CCTε antibody and immunoblotted blotted as indicated. B) The C-terminal β-propeller domain of Raptor binds to CCT. Immunoprecipitation experiments were performed with cells overexpressing the C-terminal β-propeller domain of Raptor (residues 1020-1335). C) The N-terminal region of Raptor does not bind CCT. Immunoprecipitation experiments were performed with cells over-expressing the N-terminal region of Raptor (residues 1-1019). D) Purified Raptor-CCT complex. The complex was purified using an HPC4 affinity column, concentrated, run on SDS-PAGE, stained with Coomassie and immunoblotted.

2.4.3 mTOR, Rictor, and mSIN1 do not bind to CCT

Similar to Raptor and mLST8, Rictor also has WD-40 repeats in its C-terminal region. Therefore, we wanted to know whether Rictor binds to CCT as well. mSIN1 and mTOR do not contain any domains typically recognized by CCT, and neither have been reported to interact with CCT. Nevertheless, we performed immunoprecipitations to determine whether mSIN1 and mTOR also bind CCT under the same experimental conditions we used to test Raptor-CCT interaction. We observed that Rictor does not interact with CCT despite having the WD-40 repeat domain (**Figure 2.3 B**). Moreover, mTOR and mSIN1 also showed no interaction with CCT (**Figure 2.3 A, C**). These experiments also ensured that the effects of CCT knockdowns on the assembly and signaling of mTOR complexes specifically result from an inability to fold mLST8 and Raptor.

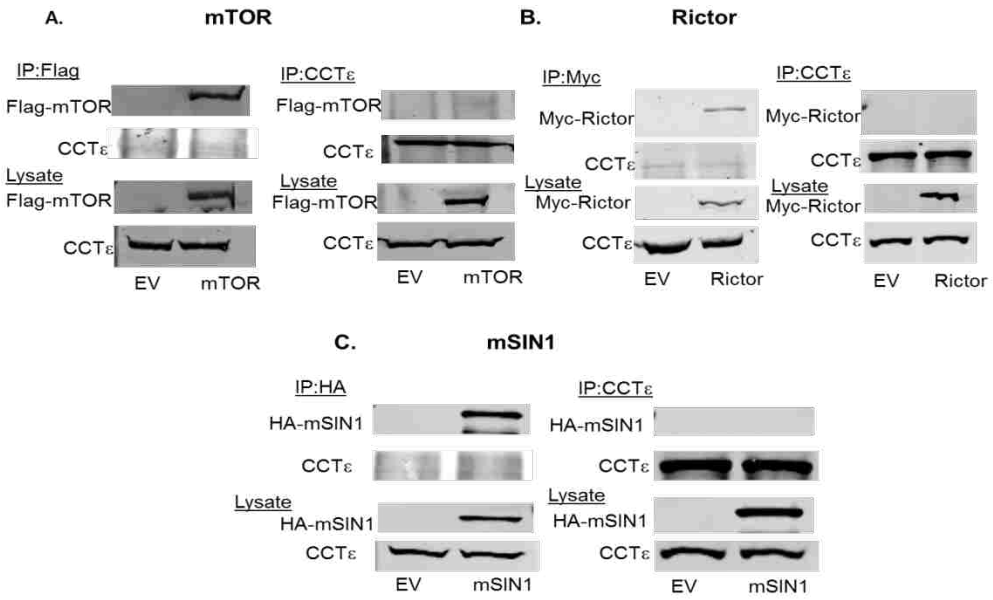

Figure 2.3 mTOR, Rictor, and mSIN1 do not interact with CCT. A) mTOR does not bind to CCT. HEK-293T cells were transfected with the Flag-mTOR or empty vector. Lysates were immunoprecipitated with a Flag antibody or a CCTε antibody and immunoblotted blotted as indicated. B) Rictor does not bind to CCT. Immunoprecipitation experiments were performed with cells overexpressing Myc-Rictor. C) mSIN1 does not bind CCT. Immunoprecipitation experiments were performed with cells over-expressing HA-mSIN1.

2.4.4 Depletion of CCT affects the endogenous expression levels of mTORC subunits.

Since we found that mLST8 and Raptor bind to CCT, we predicted that CCT folds the β-propeller domains of these proteins before they are assembled into the mTOR complexes. Appropriate folding is essential for the stability of the native protein structure. Therefore, we estimated that depletion of CCT might reduce the expression of mLST8 and Raptor as a result of their degradation caused by incorrect folding. To verify this possibility, we used two cell types, namely HEK 293T and HEPG2. In HEK 293T cells, we disrupted the CCTε gene using CRISPR methods and enriched the cells with the disruption using puromycin selection for one week. In HEPG2 cells, we transduced with a CCT shRNA virus to reduce the levels of CCT and performed puromycin selection for 3 days. We observed that HEPG2 cells were more sensitive to CCT depletion and hence were not suitable for puromycin selection over a longer period.

In 293T cells, we achieved 60-70 % knockout of CCT (**Figures 2.4 A and 2.5A**) and observed about 50% reduction in the expression of mLST8, Raptor, and mTOR in the CCT depleted cells (**Figure 2.4 A**). In contrast, the levels of Rictor and mSIN1 remained the same. We also blotted for GAPDH as a loading control to ensure both the control and CCT depleted cells had the same amount of the total protein loaded. In HEPG2 cells, a 90% CCT knockdown resulted in a 40% reduction in mLST8 levels, similar to HEK 293T cells (**Figure 2.4 B**). However, unlike HEK 293T cells, we did not see any decrease in the levels of mTOR or Raptor. A possible explanation for this result could be that HEPG2 knockdown was for a short duration as compared to HEK 293T cells. The levels of Rictor and mSIN1 remained unchanged in HEPG2 cells as in HEK 293T cells. The data from HEK293T and HEPG2 cells combined together indicate that depletion of CCT mainly affects the endogenous expression levels of

mLST8 and Raptor. Although mTOR is not a CCT substrate, its level could decrease in HEK293T cells due to its co-dependence on the presence of mLST8 and Raptor.

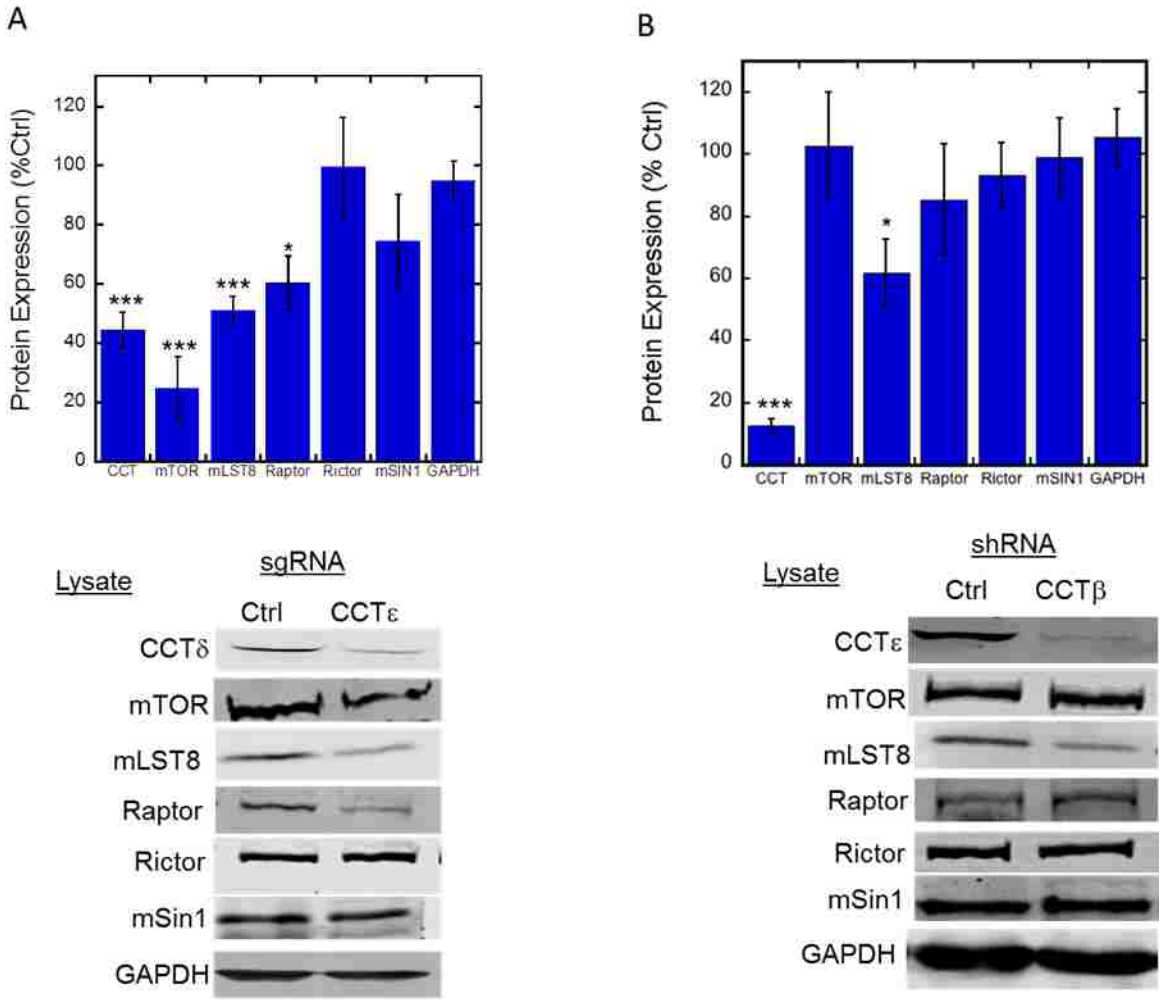

Figure 2.4 Effect of CCT depletion on the endogenous mTORC subunit expression. A) Effect of the CCT CRISPR knockout on the endogenous expression levels of mTORC components in HEK 293T cells. HEK 293T cells were transfected with control or CCT sgRNA CRISPR constructs. Cells were grown in puromycin-containing medium to select for successful knockouts. The cells were harvested after 1 week, and the lysates were blotted as shown. B) Effect of the CCT shRNA knockdown on the endogenous expression levels of mTORC components in HEPG2 cells. HEPG2 cells were transduced with viruses containing control or CCT shRNA. Cells were grown in puromycin-containing medium to select for the successful knockouts. The cells were harvested after 3 days and the lysates were blotted as shown. The bars represent averages from 5-6 experiments ± standard error. * indicates $p < 0.05$, *** indicates $p < 0.001$.

2.4.5 CRISPR knockout of CCT decreases mTORC1 and mTORC2 assembly

The finding that depletion of CCT causes a decrease in the endogenous expression of mLST8 and Raptor led us to investigate the role of CCT in mTORC assembly. To assess the same, CCT was depleted from HEK 293T cells using CRISPR techniques as described in the previous section. Both control and CCT-treated cells were transfected with the components of mTORC1 (V5-mLST8, Flag-mTOR, and HA-Raptor) or mTORC2 (V5-mLST8, HA-mSIN1, c-Myc-Rictor, and Flag-mTOR). Puromycin selection was done for 72 hours, after which the cells were harvested, and mTOR complexes were immunoprecipitated by pulling down mTOR with Flag antibody. The lysates were immunoblotted to compare the expression levels of mTORC subunits and IPs were immunoblotted to compare the extent mTORC assembly in control and CCT depleted cells. GFP was also transfected along with mTOR complexes to ensure equal transfection efficiency and specificity of the results, since GFP expression is not dependent on CCT. GAPDH was also blotted as a loading control. The CCTζ blot showed a 70% reduction in the levels of CCT in this experiment. For the mTORC1 assembly experiment, expression levels of mTOR, mLST8 and Raptor were all reduced in the CCT-depleted cells. While mTOR expression was moderately reduced by about 20%, mLST8 and Raptor expression showed a significant reduction of about 50% with CCT depletion. A similar trend was reflected in the IPs which showed 30% decrease in mTOR, a 50% decrease in mLST8, and a 30% decrease in Raptor, which is somewhat lower than the 50% decrease in Raptor expression.

With the mTORC2 assembly experiment, mTOR showed a modest decrease in both expression (30 %) and immunoprecipitation (20 %), whereas mLST8 showed greater decreases in both expression (40 %) and immunoprecipitation (50 %). mSIN1 and Rictor expression levels did not change, and their co-immunoprecipitations with mTOR showed modest decreases of 30%

for mSIN1 and 20% for Rictor, which can be attributed to the decrease in mTOR immunoprecipitation. The levels of GFP and GAPDH remained constant even after CCT depletion for both the mTORC1 and mTORC2 assembly, indicating that the effects observed were specifically due to the absence of CCT. Collectively, these data indicate that CCT plays a role in the formation of the mTOR complexes. mLST8 is dependent on CCT for its assembly into both mTORC1 and mTORC2, while Raptor is dependent on CCT for its assembly into mTORC1. However, mSIN1 and Rictor do not require CCT for their assembly into mTORC2.

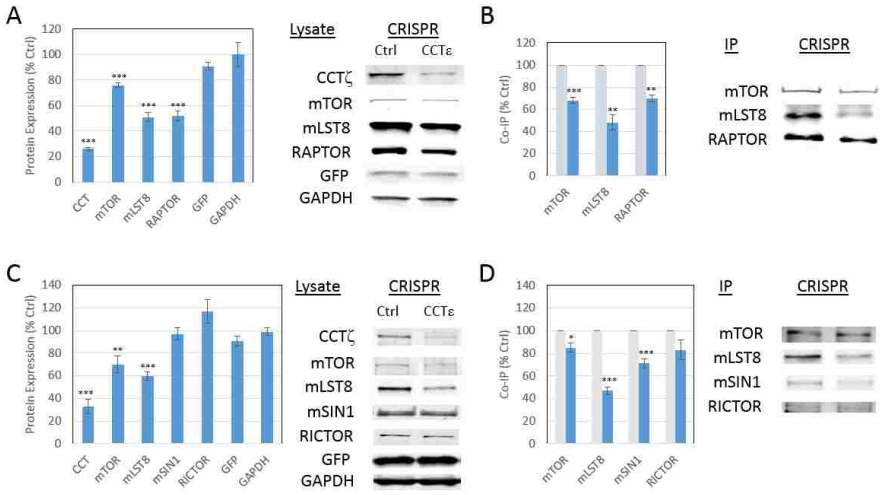

Figure 2.5 The effects of CRISPR depletion of CCT on the assembly of mTOR complexes. Effects of CRISPR-mediated CCT depletion on mTORC1 subunit expression. HEK-293T cells were treated with CCTε sgRNA along with Cas9 and transfected with c-Myc-mTOR, V5-mLST8, HA-Raptor, and GFP. mTORC1 components in the cell lysates were immunoblotted as indicated. The graph shows the relative expression level compared to control cells with non-targeting sgRNAs. B) Effects of CRISPR-mediated CCT depletion on mTORC1 assembly. c-Myc-mTOR was immunoprecipitated from the lysates and immunoblotted for c-Myc-mTOR, V5-mLST8 and HA-Raptor to assess the level mTORC1 assembly. The graph shows the relative co-immunoprecipitation of mTORC1 subunits compared to the non-targeting sgRNA control. C) Effects of CRISPR-mediated CCT depletion on mTORC2 subunit expression. Cells were treated with CCTε sgRNA along with Cas9 and transfected with Flag-mTOR, V5-mLST8 and HA-mSIN1, c-Myc-Rictor, and GFP. mTORC2 components in the cell lysates were immunoblotted as indicated. The graph shows the relative expression level compared to control cells with non-targeting sgRNAs. D) Effects of CCT depletion on mTORC2 assembly. Flag-mTOR was immunoprecipitated from the lysates and immunoblotted for Flag-mTOR, V5-mLST8, HA-mSIN1, and c-Myc-Rictor to assess the level mTORC2 assembly. The graph showed the co-immunoprecipitated mTORC2 components with the CRISPR knockdown by CCT sgRNA compared to the non-targeting sgRNA control. Bars in the graphs represent the average ± standard error from at least three biological replicates. * indicates $p < 0.05$. ** indicates $p < 0.01$. *** indicates $p < 0.001$.

2.4.6 siRNA knockdown of CCT decreases mTORC1 and mTORC2 assembly

Parallel to CRISPR knockdown, we also did siRNA mediated knockdown of CCT to assess its effect on the assembly of mTOR complexes. In HEK 293T cells, knockdown of CCT was done with siRNAs targeting to α and ε subunits of CCT, followed by transfection of mTORC1 (V5-mLST8, Myc-mTOR, and HA-Raptor) or mTORC2 (V5-mLST8, HA-mSIN1, c-Myc-Rictor, and Flag-mTOR). Cells were harvested 96 hours after knockdown, and mTOR complexes were immunoprecipitated by pulling down c-Myc-mTOR for mTORC1 or Flag-mTOR for mTORC2. The lysates and IPs were immunoblotted to determine the change in the expression levels and assembly respectively. This siRNA experiment showed a similar trend in the expression and assembly of mTORC1 as that of the CRISPR method. With 70 % CCT knockdown, expression of mTOR, mLST8, and Raptor were reduced by 35 % - 40 %. In the case of IP, mTOR was down by 50 %, mLST8 by 40 %, while Raptor showed a larger 70 % reduction.

In the case of mTORC2, mTOR and mSIN1 expression and IP did not change with CCT knockdown. mLST8 expression was reduced significantly by 50% with about 40% decrease in its assembly. However, unlike the CRISPR method, Rictor expression and assembly increased by about two-fold with CCT knockdown. Despite some differences in the results, the effects of siRNA knockdown on mTORC1 and mTORC2 assembly showed a comparable trend to the CRISPR method reinforcing the fact that CCT is involved in the assembly of mTOR complexes by means of mLST8 and Raptor folding.

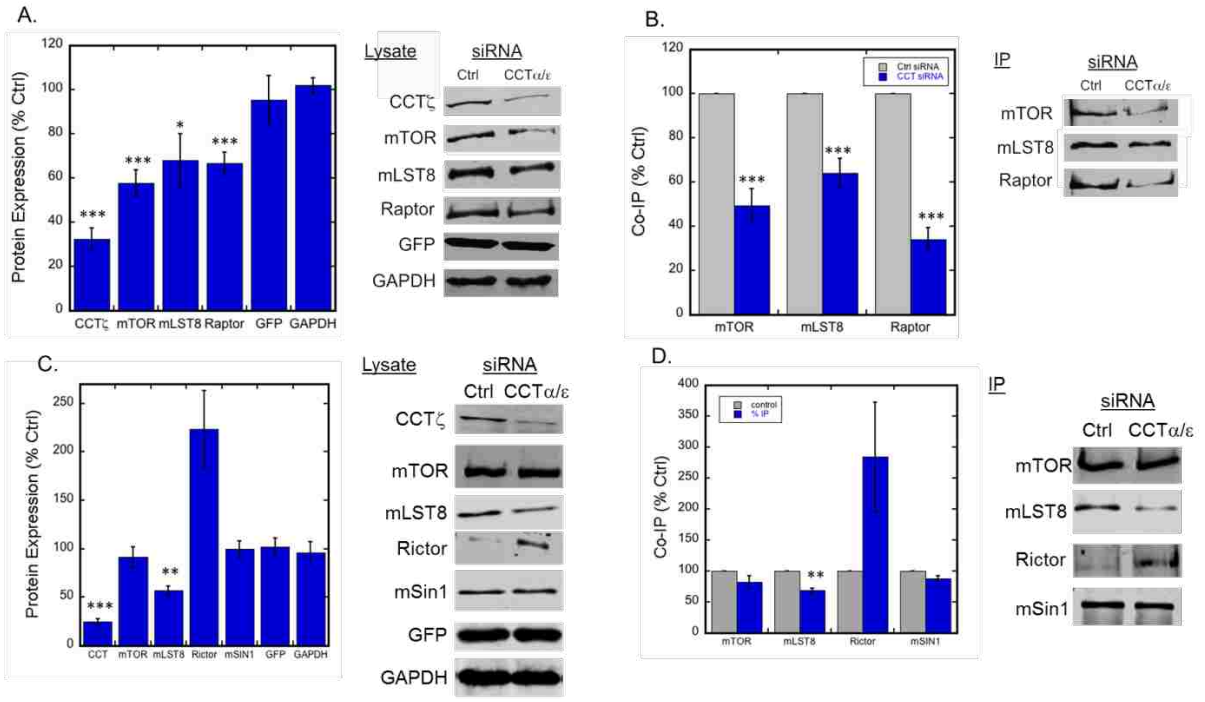

Figure 2.6 The effects of siRNA knockdown of CCT on the assembly of mTOR complexes A) Effects of CCT depletion on mTORC1 subunit expression. HEK-293T cells were treated with CCTα and CCTε siRNAs or a non-targeting siRNA and transfected with mTOR, mLST8, Raptor, and GFP. Lysates were immunoblotted as shown. Bars represent the average ± standard error from at least four experiments. * indicates $p < 0.05$, ** $p < 0.005$, *** $p < 0.001$. B) Effects of CCT depletion on mTORC1 assembly. mTOR was IPed from lysates and immunoblotted for mTOR, mLST8 and Raptor to assess the level mTORC1 assembly. The graph shows the co-IP, comparing CCT siRNA to the control. Bars represent the average ± standard error from 15 experiments. C) Effects of CCT depletion on mTORC2 subunit expression. Cells were treated with siRNAs as in A and transfected with mTOR, mLST8, Rictor, mSIN1, and GFP. Lysates were immunoblotted as shown. Bars represent the average ± standard error from six experiments. D) Effects of CCT depletion on mTORC2 assembly. mTOR was IPed from lysates and immunoblotted for mTOR, mLST8, Rictor and mSIN1 to assess the level mTORC2 assembly. The graph shows the co-IP, comparing CCT siRNA to the control. Bars represent the average ± standard error from six experiments.

2.4.7 Stability of newly synthesized mLST8 is highly dependent on CCT

CCT deprivation does not affect the pre-assembled mTOR complexes which are stable for a long period of time, explaining why the endogenous mLST8 did not decrease by more than 50% even after 90% depletion of CCT. Moreover, CRISPR or siRNA methods achieved 70% decline in CCT which may not be sufficient to degrade the over-expressed mLST8 by more than 50%. To address these issues, we turned to Hap1 cells in which endogenous mLST8 has been

CRISPR deleted to test the effects of CCT depletion on the newly synthesized mLST8. **Figure 2.6** shows wild type Hap1 cells and the isotype matched mLST8 knockout cells, indicating that the knock-out was successful. We then transduced exogenous mLST8 into the mLST8 knockout cells, followed by treatment with control or CCT shRNA. While the mLST8 expression was restored in the cells with control shRNA (**Figure 2.6)**, it was severely reduced by about 70%-80% in the CCT depleted cells. These results indicate that newly synthesized mLST8 is not stable in the cells lacking CCT.

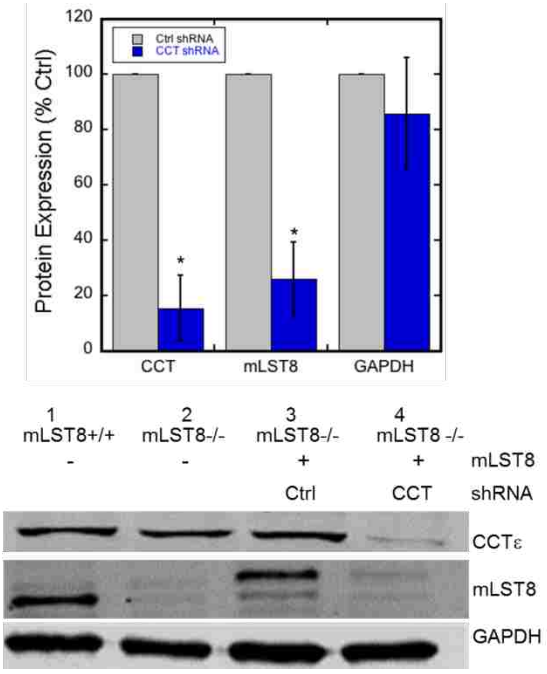

Figure 2.7 Expression of newly synthesized mLST8 is highly dependent on CCT. mLST8 deleted cells were transduced with a virus containing C-term V5 tagged mLST8 and selected with blasticidin, followed by transduction with control or CCT shRNA within 24 hours. The cells were grown 2.5 days after CCT depletion, harvested and immunoblotted as indicated above. Lane1: Hap1 wild type, Lane 2: Hap1 with mLST8 knockout. Lane3: mLST8 knockout transduced with mLST8-V5 cDNA and control shRNA. Lane 4: mLST8 knockout transduced with mLST8-V5 cDNA and CCT shRNA. The graph represents CCT, mLST8, and GAPDH levels in lane 4 as compared to lane 3. The bars represent average ± standard error from 3 experiments. * represents $p < 0.05$.

2.4.8 siRNA knockdown of PhLP1 causes a reduction in the mTORC1 assembly.

With the importance of CCT for mTORC assembly established, we turned our attention to study the role of PhLP1 in the same context. Therefore, we measured the effects of siRNA depletion of PhLP1 on mTORC1 assembly in HEK 293T cells as we had for CCT.

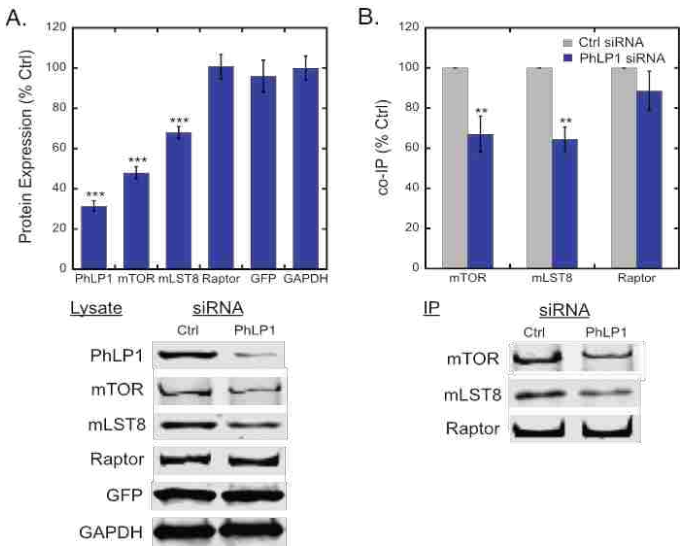

Figure 2.8 siRNA knockdown of PhLP1 affects mTORC1 assembly. A) Effects of PhLP1 depletion on mTORC1 subunit expression. HEK-293T cells were treated with PhLP1 or a non-targeting control siRNA and transfected with Myc-mTOR, Flag-mLST8, and HA-Raptor. Lysates were immunoblotted as shown. Bars represent the average ± standard error from nine experiments. *** indicates $p < 0.001$. B) Effects of PhLP1 depletion on mTORC1 assembly. mTOR IPs and blots were performed as in Fig. 2.6B. The graph shows the average ± standard error from 7-9 experiments. ** indicates $p < 0.01$.

As compared to control cells, expression of mLST8 and mTOR were reduced by 35 % and 50 % respectively with a PhLP1 knockdown. However, PhLP1 knockdown did not cause a decrease in Raptor expression. Similarly, IPs of mTOR and mLST8 were reduced by 40% while Raptor IP remained the same, indicating that PhLP1 contributes to mLST8 folding and assembly with mTOR, but it is not required for Raptor folding.

2.4.9 Effects of CCT and PhLP1 knockdowns on the mTOR signaling.

Since CCT and PhLP1 are important for the integrity of mTOR complexes, we reasoned that their depletion would show negative effects on the mTOR signaling. To test this hypothesis, CCT and PhLP1 were knocked down in HEPG2 cells for total 96 hours. The cells were serum starved overnight before harvest and were stimulated with 1 μM insulin for 30 minutes or 50 nM insulin for 10 minutes to activate mTORC1 or mTORC2, respectively (**Figure 2.8A**). Simultaneously, mLST8 and Raptor knockdowns were used as positive controls. Cell lysates were blotted for of p-IRS$^{S636/639}$ to measure mTORC1 signaling and p-AKT^{S473} to measure mTORC2 signaling.

CCT deprived cells showed a 40% reduction in both the p-IRS1 and p-AKT, (**Figure 2.9A**). This decrease is similar to that seen in mLST8 depleted cells, which showed a 60% reduction in the p-AKT levels and a 40% reduction in the p-IRS1 levels. Raptor depletion also caused a similar decrease in p-IRS-1 level, but did not change p-AKT levels as expected for a subunit of mTORC1. These results are consistent with the finding that CCT is required for the assembly of mTORC1 and mTORC2. In the case of PhLP1, its depletion caused a 60% reduction in the p-AKT (**Figure 2.9A**) which is consistent with the idea that PhLP1 could be a co-chaperone for folding of mLST8. However, PhLP1 depletion caused a marginal increase in p-IRS1 levels. This result is in line with the lack of effect of PhLP1 depletion on mTORC1 assembly (**Figure 2.8**).

To confirm the CCT siRNA effects on mTOR signaling, we depleted CCT from HEPG2 cells with a CCTβ shRNA as described in Figure 2.4B and measured the phosphorylation of mTOR substrates. shRNA depletion of CCT decreased the levels of p-S6K1 by 50%, p-S6 by

70%, and p-AKT by 40%, confirming the siRNA results and underlining the importance of CCT for mTORC1 and mTORC2 signaling.

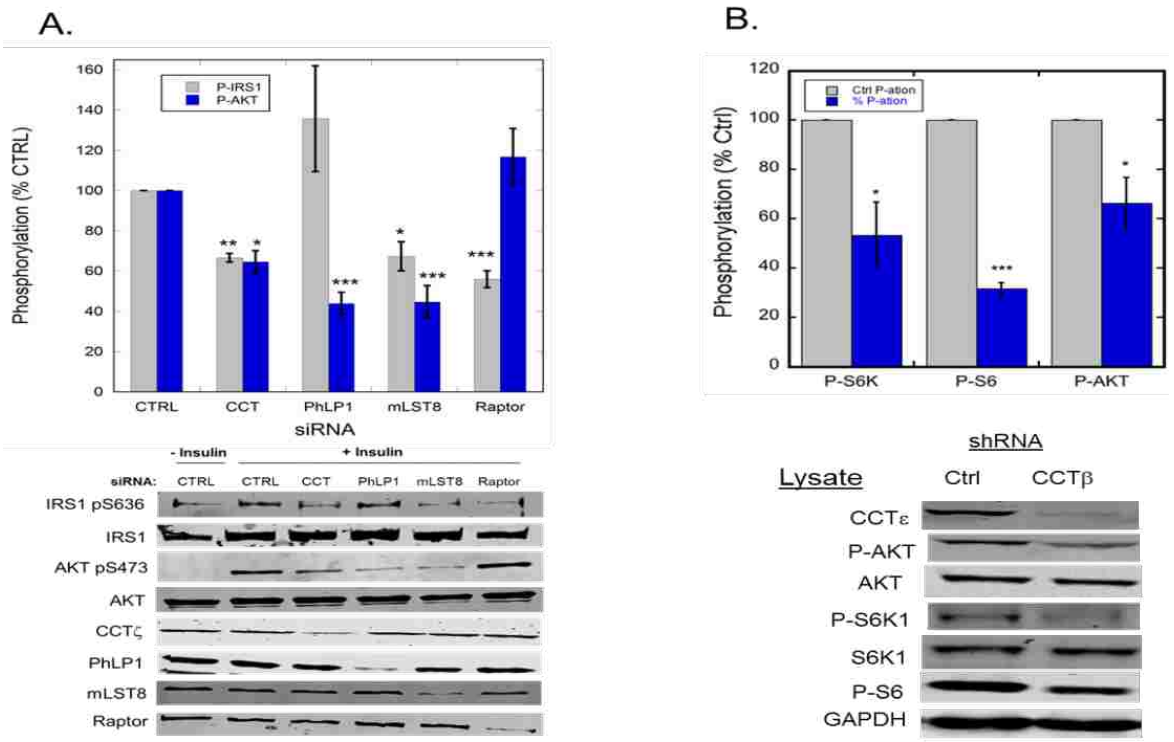

Figure 2.9 Effects of CCT and PhLP1 knockdown on mTOR signaling A) HEPG2 cells were treated with siRNAs to CCTα and CCTε, PhLP1, mLST8 or Raptor as indicated. The cells were serum-starved overnight and treated with 1 μM insulin for 30 minutes to activate mTORC1 or 50 nM insulin for 10 minutes to activate mTORC2. The effects on mTORC1 and mTORC2 signaling were determined by immunoblotting the cell lysates for IRS1 pS636 and AKT pS473, respectively. The lysates were also immunoblotted to assess the respective knockdowns and total AKT and IRS1 levels. Representative blots are shown. The graph represents average ± standard error from 3-7 experiments. * indicates $p < 0.05$, ** $p < 0.005$, *** $p < 0.001$. B) HEPG2 cells were treated with control or CCT shRNA as described in Figure 2.3B and the lysates were immunoblotted for AKT pS473, S6K1 pT389, and S6 pS236. The graph represents average ± standard error from 5-6 experiments. * indicates, p *** $p < 0.001$.

2.4.10 Structural analysis of mLST8-CCT and PhLP1-mLST8-CCT complexes

Since mLST8 was found to interact with CCT and PhLP1, we wanted to obtain structural information of their interactions to reveal the mechanism of mLST8 folding. Hence, we purified

mLST8-CCT and PhLP1-mLST8-CCT from HEK 293T cells as described in the experimental procedures (**Figure 2.10**). The purified complexes were then sent to the laboratory of Jose Valpuesta at the Centro Nacional de Biotecnologia in Madrid, Spain for cryo-EM analysis.

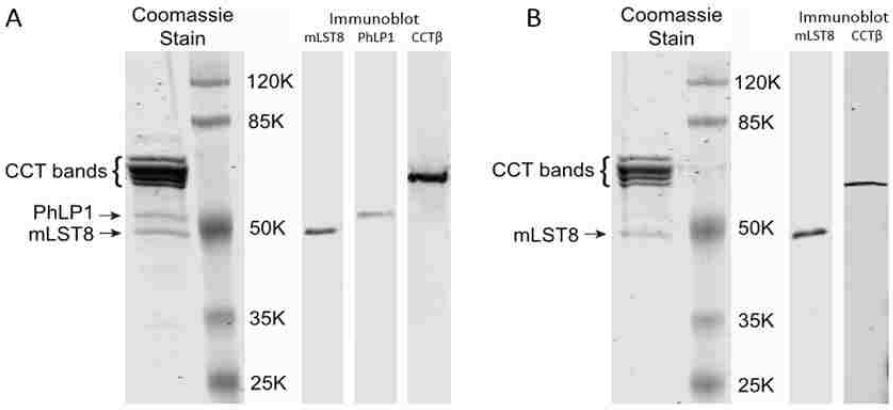

Figure 2.10 Purification of mLST8-CCT and PhLP-mLST8-CCT complexes A) PhLP1-mLST8-CCT, B) mLST8-CCT. The complexes were purified by cobalt-Strep tandem affinity purification. The concentrated protein complexes were run on SDS-PAGE, stained with Coomassie blue and immunoblotted as indicated. The Coomassie-stained gels show the purity of the complexes and the immunoblots identify the mLST8, PhLP1 and CCTβ bands.

As indicated by the 2D-reconstructions, we have successfully obtained a homogeneous population of particles for both the mLST8-CCT and PhLP1-mLST8-CCT complexes (**Figure 2.11**). Class averages of these structures showed the typical double-stacked 8-membered ring structure of CCT with a mass inside the cavity in the mLST8-CCT complex and a mass above the cavity for the PhLP1-mLST8-CCT complex. We went on to perform a high resolution cryo-EM analysis of the mLST8-CCT complex and picked 315,866 particles for 2-D class averages, which showed some apo-CCT and mLST8 bound CCT particles. A 3-D reconstruction of the mLST8-CCT particles yielded an 8Å resolution structure which revealed that mLST8 is buried deep inside the folding cavity of CCT (**Figure 2.11C**).

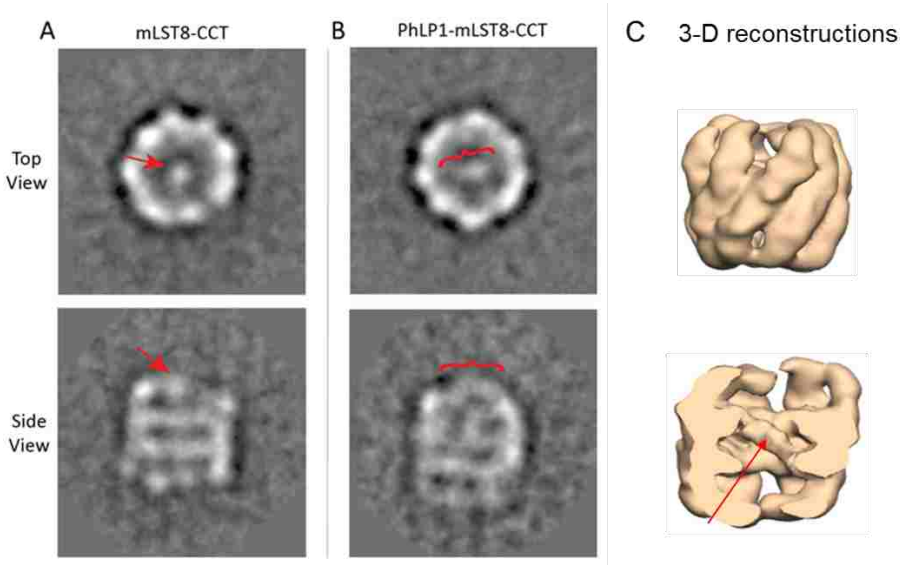

Figure 2.11 Cryo-EM analysis of mLST8-CCT and PhLP-mLST8-CCT complexes A) Images of cryo-EM class-averages of the mLST8-CCT complex. Top and side view images show a mass inside the CCT cavity attributable to mLST8 (red arrows). B) Images of cryo-EM class-averages of the PhLP1-mLST8-CCT. Top and side views of this complex show a mass attributable to PhLP1 spanning the top of CCT folding cavity (red brackets). C) Cryo-EM reconstruction of the mLST8-CCT complex. A cut away image reveals that a mass of mLST8 is located in the deep inside of the CCT cavity.

2.4.11 XL-MS analysis of mLST8-CCT

We also analyzed the purified mLST8-CCT complex by cross-linking coupled with mass spectrometry. The purified mLST8-CCT was treated with disuccinimidyl suberate (DSS) as a crosslinker followed by size exclusion chromatography to enrich the cross-linked samples which were identified by mass spectrometry. XL-MS yielded some intra-protein as well as inter-protein crosslinks. The inter-protein crosslinks provided distance constraints to map mLST8 within the cryo-EM density. We obtained seven intra-protein crosslinks of mLST8 and three inter-protein crosslinks between mLST8 and CCT (**Figure 2.12C**). The available crystal structure of the mTOR-mLST8 complex was used as a reference to map the intra-protein crosslinks of mLST8.

Out of the seven intra-protein crosslinks, six were below the maximum limit of 35 Å, while one of them mapped to 37 Å. This observation indicated that mLST8 had reached a near-native conformation in the substrate cavity.

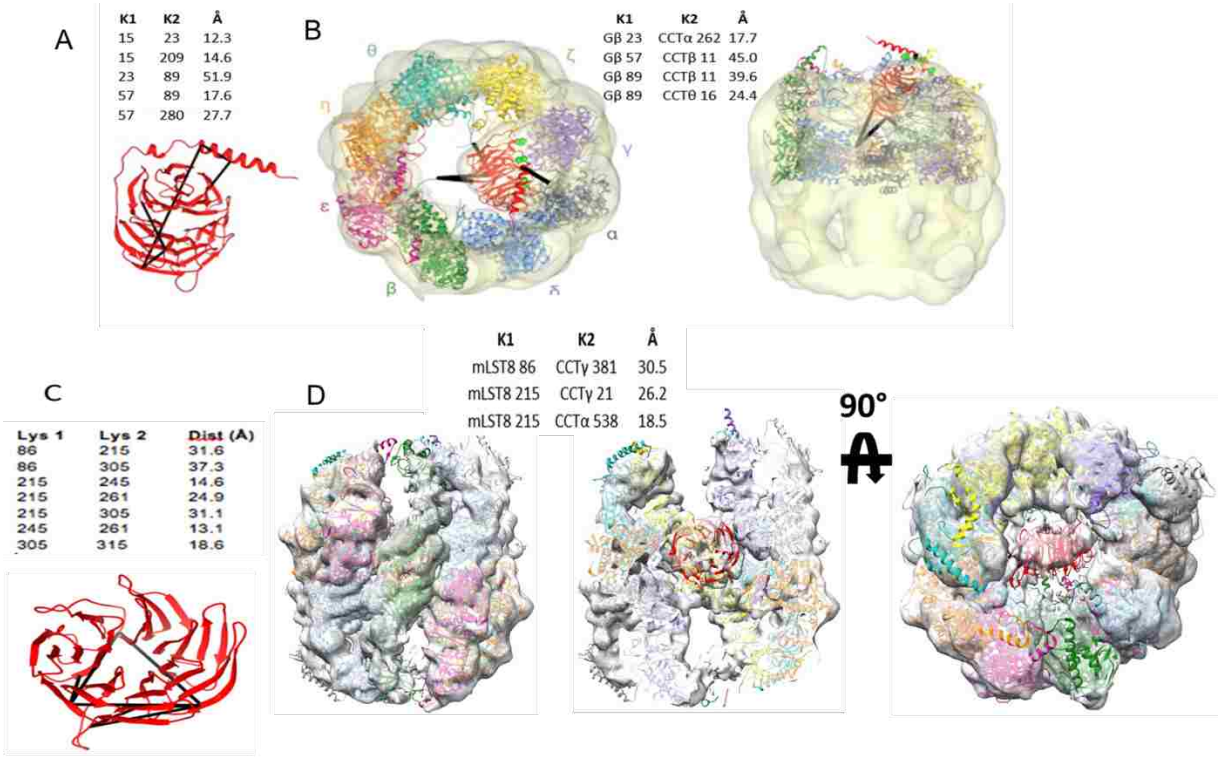

Figure 2.12 Structural comparison between Gβ-CCT and mLST8-CCT. A) Gβ structure is meta-stable when bound to CCT. Cross-linking coupled with mass spectrometric identification (XL-MS) of intra-molecular Gβ cross-links. Distances longer than 35 Å indicate deviations from the fully folded structure. B) Gβ-CCT structure. Docking of CCT and Gβ into the cryo-EM volume of Gβ-CCT guided by XL-MS and unnatural amino acid cross-links. Gβ is positioned high in the CCT cavity near CCTα and CCTγ. [50] C) mLST8 is more stable when bound to CCT. XL-MS of intra-molecular mLST8 cross-links. D) mLST8-CCT structure. Several views of the mLST8-CCT complex (side, side cut away, and end-on). The cryo-EM electron density at 7.4 Å resolution is shown with the atomic structures of CCT (5GW4), and mLST8 (4JT6, red) docked into the density. mLST8 is positioned at the bottom of the cavity between the two CCT rings.

One of the three inter-protein crosslinks was formed between K86 of mLST8 and K381 of CCTγ, whereas K215 of mLST8 was crosslinked alternatively to K21 of CCTγ and K538 of

CCTα (**Figure 2.11 D).** These crosslinks are found in the bottom of the CCT folding cavity, confirming the position of mLST8 observed in the cryo-EM structure and indicating that mLST8 contacts CCTα and CCTγ.

2.4.12 Raptor binds to PhLP1

The observed interaction between Raptor and CCT raised the question whether Raptor also binds to PhLP1. To address this question, we co-transfected myc-PhLP1with either empty vector or HA-Raptor in HEK 293T cells. Raptor was immunoprecipitated with HA antibody and the myc-PhLP1 band was observed in the co-IP indicating that Raptor interacts with PhLP1 (**Figure 2.13 A**). Alternatively, we pulled down myc-PhLP1 as a primary IP and observed HA-Raptor as a co-IP (**Figure 2.13 A**). We also tested which domain of Raptor binds to PhLP1 by doing immunoprecipitations of PhLP1 with Raptor truncations. We observed that PhLP1 interacts with the C-terminal WD-40 repeats of Raptor very strongly as compared to the N-terminal domains (**Figure 2.13B, C**). Next, we wanted to know whether Raptor forms a ternary complex with PhLP1 and CCT similar to Gβ. Therefore, we tested the effect of CCT depletion on PhLP1-Raptor interaction and observed that the amount Raptor co-IP with PhLP1 increases by more than 2-fold with CCT knockdown (**Figure 2.12 D**). These data suggest that Raptor binds to PhLP1 independent of CCT, and that PhLP1 and CCT may also compete with each-other for binding to Raptor.

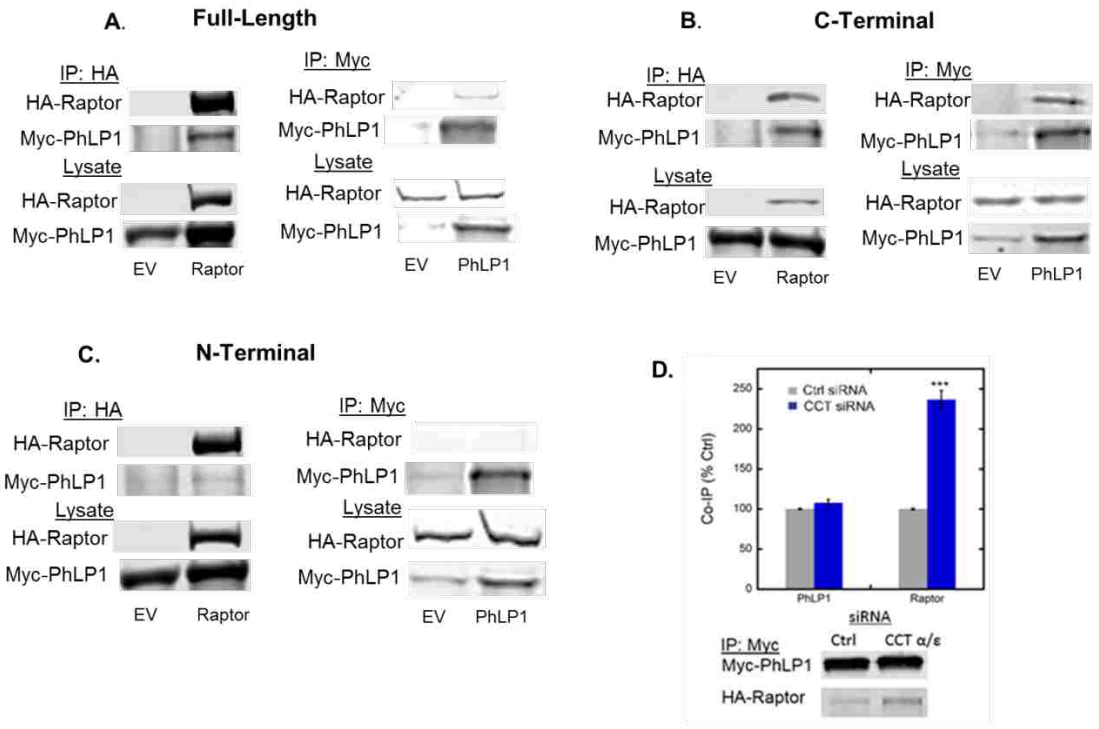

Figure 2.13 PhLP1 binds to Raptor A) Full-length Raptor interacts with PhLP1. Immunoprecipitation experiments were performed with cells with over-expressing empty vector (EV) and HA-Raptor or EV and Myc-PhLP1. Lysates were immunoprecipitated with HA or Myc antibody and immunoblotted as indicated. B) C-terminal Raptor interacts with PhLP1. Immunoprecipitations were done with cells overexpressing C-terminal Raptor and PhLP1. C) N-terminal Raptor interacts with PhLP1 very weakly. Immunoprecipitations were done with cells overexpressing N-terminal Raptor and PhLP1. D) CCT depletion increases PhLP1 binding to Raptor. The PhLP1-Raptor co-immunoprecipitation experiment was performed with cells treated with control siRNAs or CCT siRNA. The graph shows the protein in the immunoprecipitate from CCT siRNA treated cells compared to control cells. Bars represent the average ± standard error from three experiments. *** $p < 0.001$.

2.4.13 PhLP1 depletion causes an increase in Raptor expression

Since we identified an interaction between PhLP1 and Raptor, we wanted to test the effects of PhLP1 depletion on Raptor expression. Therefore, we used a HEK 293T cell line in which PhLP1 was CRISPR deleted. We compared the amount of endogenous Raptor in the wild-type and PhLP1 knockout cells by immunoblotting. PhLP1 knockout cells showed a small but significant 40% increase in endogenous Raptor expression. We also compared the levels of

endogenous mLST8 in wild-type and PhLP1 knockout cells and observed that they remained the same.

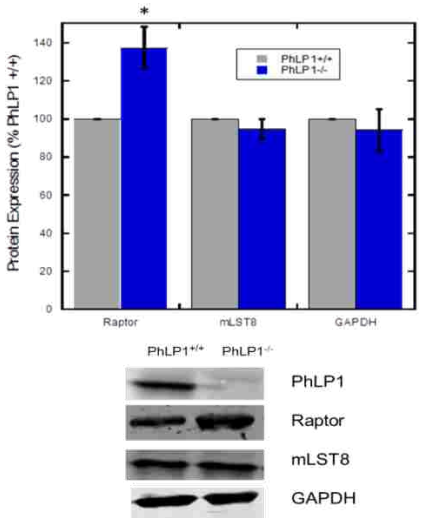

Figure 2.14 Raptor expression is increased in the cells with PhLP1 knockout Wild-type or PhLP1 knockout HEK 293T cells were lysed and immunoblotted for endogenous Raptor, mLST8, and GAPDH. * indicates $P < 0.05$

2.4.14 PhLP1 facilitates Raptor ubiquitination and degradation

PhLP1 seemed to play a different role in the case of Raptor as compared to mLST8, in which it was a part of a ternary complex with CCT. Therefore, we further explored the role of PhLP1 regarding the function of Raptor. Raptor was overexpressed in the cells treated with either control or PhLP1 siRNA and Raptor levels were assessed by immunoblotting. Raptor expression increased by 3-fold in the PhLP1 deprived cells (**Figure 2.15**), indicating that PhLP1 may contribute to the degradation of Raptor. To assess this possibility, we tested the effects of PhLP1 depletion on Raptor ubiquitination. We overexpressed Raptor and HA-ubiquitin in the HEK 293T cells treated with PhLP1 siRNA. The cells were further treated with MG132, a proteasome inhibitor for 2-4 hours before the harvest. Ubiquitin was pulled down with HA antibody, and the immunoprecipitates were blotted for HA. We observed a smear-like pattern on

the HA blot near the molecular weight of Raptor, indicating that Raptor was poly-ubiquitinated. Also, the poly-ubiquitination showed a 40% reduction in the PhLP1 depleted cells, indicating that PhLP1 contributes to the degradation of Raptor.

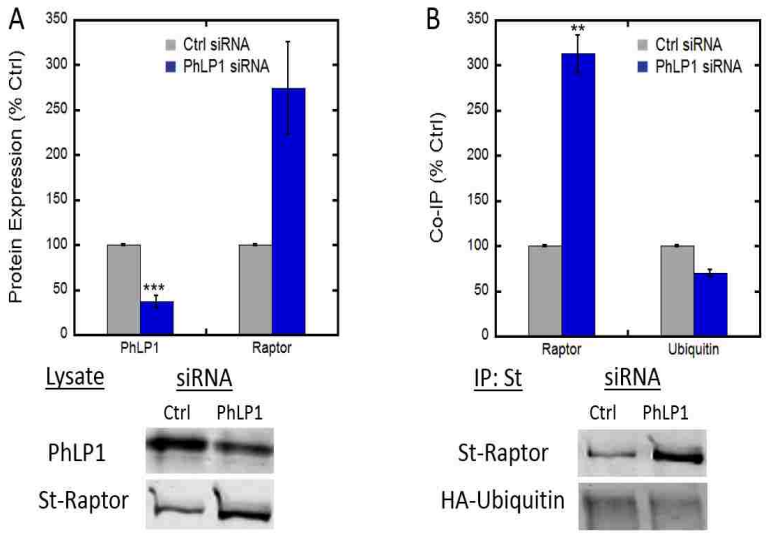

Figure 2.15 PhLP1 contributes to degradation of Raptor A) Effects of PhLP1 knockdown on Raptor expression and ubiquitination. HEK-293T cells were treated with PhLP1 siRNA or a non-targeting control siRNA, and cell lysates were immunoblotted as shown. B) PhLP1 contributes to Raptor ubiquitination. HEK-293T cells were treated with PhLP1 siRNA or a non-targeting control siRNA, followed by co-transfection with Strep-Raptor and HA-ubiquitin. The cells were treated with 10 μM of the proteasome inhibitor MG-132 2-4 hours prior to harvest. Raptor was immunoprecipitated from the lysates and immunoblotted for HA-ubiquitin. Bars represent the average ± standard error from 5-6 experiments. ** indicates $p < 0.02$. *** indicates $p < 0.001$.

2.4.15 mTORC1 signaling is elevated in PhLP1 deprived cells

Since PhLP1 depletion was shown to stabilize Raptor, we wanted to further study its effects on mTORC1 signaling. Therefore, we compared mTORC1 signaling in the wild-type and PhLP1 CRISPR-deleted HEK-293T cells. These cells were serum starved overnight, treated with insulin and blotted for p-S6K1 to measure mTORC1 signaling and p-AKT to measure mTORC2 signaling. We saw a significant 50 % increase in p-S6K1 in the PhLP1 knockout cells, which is consistent with the observed increase in Raptor expression in these cells and the increase in p-

IRS-1 observed in PhLP1 siRNA-treated HEPG2 cells. In contrast, p-AKT did not show the same decrease observed in PhLP1 siRNA-treated HEPG2 cells, suggesting that insulin-mediated mTORC2 activity in HEK-239T cells is less dependent on PhLP1.

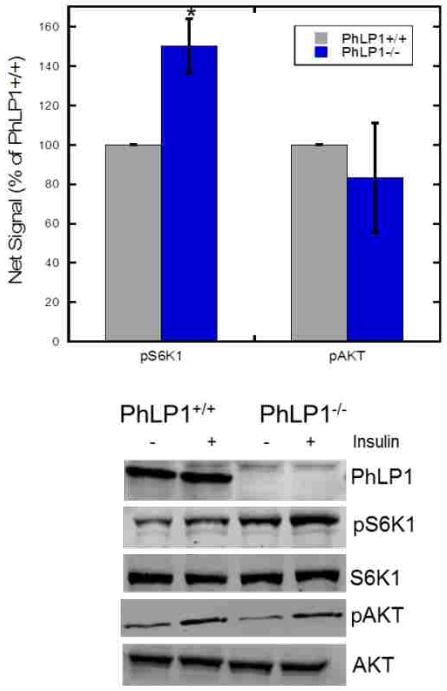

Figure 2.16 Effects of PhLP1 depletion on mTOR signaling Control or PhLP1 deleted (-/-) HEK-293T cells were grown to the same confluency. The cells were serum-starved overnight and stimulated with 2 nM insulin for 30 minutes. The lysates were immunoblotted for PhLP1, S6K1pT389, AKTpS473, total S6K1, and total AKT. For each cell type, the extent of insulin stimulation is measured by calculating the fold increase in phosphorylation. The graph represents averages ± standard error from 3-4 experiments. * represents $p < 0.05$.

2.5 Discussion

2.5.1 CCT as a chaperone for mLST8 and Raptor

Our studies point to an important role for the cytosolic chaperonin in mTOR signaling by folding two of the mTORC components, mLST8 and Raptor. Initially, we identified a direct

interaction between mLST8-CCT and Raptor-CCT by co-immunoprecipitations. Next, we showed that depletion of CCT reduces the endogenous as well as over-expressed levels of mLST8 and Raptor and hence also affects the assembly of mTORC1 and mTORC2. Interestingly, some of the experiments also showed a reduction in mTOR levels between 30-50 %, even if it doesn't require CCT for its folding. However, this observation is not surprising as mLST8 is required for stabilization of mTOR. Another important observation is that the expression of both mLST8 and Raptor, whether endogenous or overexpressed, always showed a partial decrease (between 30%-50%) with CCT knockdown. It can be explained by the fact that the pre-formed endogenous complexes are highly stable and a 70% CCT knockdown is not sufficient to drastically affect the over-expressed complexes. To address the issues of partial effects, we supplied exogenous mLST8 to the mLST8-/- cells and observed a severe reduction in its expression when CCT was knocked down. Finally, we did signaling experiments and observed that CCT deprivation also has a negative impact on mTORC1 and mTORC2 signaling. Combined together, these observations lead to a conclusion that CCT acts as a chaperone for mLST8 and Raptor by folding their β-propeller domains and thus is critical for the structural integrity of the mTOR complexes.

2.5.2 Structural comparison of Gβ-CCT and mLST8-CCT complexes

Cryo-EM combined with XL-MS analysis of the mLST8-CCT structure showed that mLST8 sits deep within the folding cavity of CCT and contacts CCTα and CCTγ subunits. When compared with the Gβ-CCT structure, we found that Gβ is positioned very differently at the top of the CCT folding cavity. The position of Gβ high inside CCT allows it to interact with PhLP, which is required to complete the process of Gβ folding and its release for interaction with the G

protein γ subunit [50]. In contrast, mLST8 is not accessible to PhLP1 in its position buried inside CCT. Although PhLP1 is found to be a part of the ternary complex with mLST8 and CCT, its role as a co-chaperone could be different in case of mLST8 as compared to Gβ.

Importantly, the intra-protein crosslinks of mLST8 indicate that it has achieved a near-native structure. Moreover, cross-links with CCTγ and CCTα indicate that mLST8 is positioned on the side of CCT with weaker ATPase activity that is possibly the preferential site for the release of substrate. These observations indicate that mLST8 in the isolated complex has achieved a near-native state and is ready for release into cytosol.

2.5.3 The scheme of CCT-dependent assembly of the mTOR complexes and PhLP1 mediated degradation of Raptor

Based on our studies, we propose a model for the assembly of mTOR complexes. The nascent polypeptides of mLST8 and Raptor are folded into their native structures inside the folding cavity of CCT. The correctly folded mLST8 is then assembled into mTORC1 or mTORC2, whereas folded Raptor assembles into mTORC1. However, it is not clear if mLST8 and Raptor are stable until they find their binding partners or whether they require other chaperones to assist their entry into the functional mTOR complexes. Further studies are required to understand how mLST8 and Raptor get into mTORC1 or mTORC2 after their release from CCT and also to determine the exact role of PhLP1 in case of mLST8 and Raptor folding.

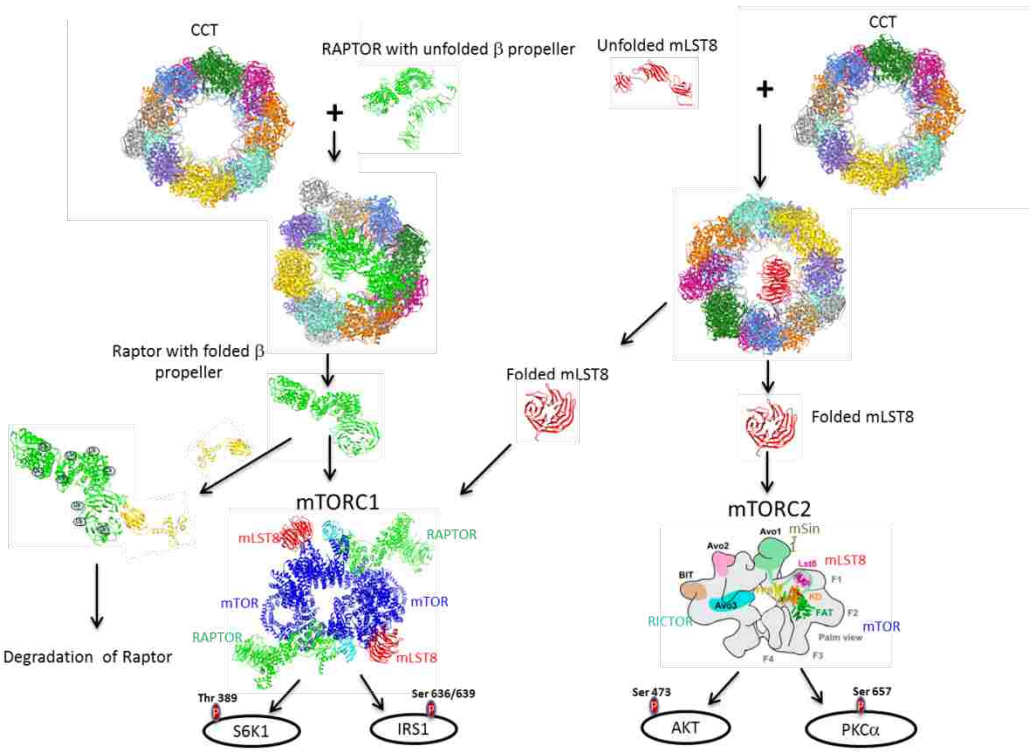

Figure 2.17 The role of CCT and PhLP1 in mTORC assembly and signaling. Nascent polypeptides of mLST8 and CCT are entrapped inside CCT. CCT folds mLST8 which interacts with mTOR and Raptor for its assembly into mTORC1. Alternatively, mLST8 interacts with mSIN1 and mTOR for its assembly into mTORC2. The C-terminal domain of Raptor is folded by CCT, which then assembles into mTORC1. PhLP1 binds to the C-terminal of Raptor and facilitates its degradation. CCT is thus required for the structural integrity of the mTOR complexes which can then participate in downstream signaling.

2.5.4 Role of PhLP1 as a co-chaperone for mLST8 and Raptor

Our studies have revealed that the role of PhLP1 is very diverse with respect to folding of mLST8 and Raptor. The positioning of mLST8 at the bottom of the CCT folding cavity indicates that unlike Gβ, PhLP1 may not be required for release of mLST8 from CCT. PhLP1 depletion decreased the levels of over-expressed mLST8, indicating that it is involved in mTORC1 assembly. However, we did not observe the same effects on the endogenous mLST8 levels in PhLP1-deleted cells. Moreover, PhLP1-deleted cells did not show any effect on mTORC2 signaling. However, we saw a clear interaction between mLST8 and PhLP1 by co-immunoprecipitations and also identified the formation of a PhLP1-mLST8-CCT complex.

These findings indicate that expression of mLST8 may not be absolutely dependent on PhLP1 but it could still play some role as a co-chaperone and hence more studies investigating the role of PhLP1 with respect to mLST8 are required. We have also shown a possible new function of PhLP1 in degradation of Raptor. PhLP1 depletion caused an increase in Raptor expression both at the endogenous and over-expressed levels. Raptor ubiquitination was also reduced with PhLP1 deprivation. Moreover, mTORC1 signaling was found to be elevated in PhLP1-depleted cells possibly as an indication of Raptor stabilization. These data indicate that PhLP1 could facilitate degradation of Raptor. We have also shown that PhLP1 interacts with Raptor independent of CCT and hence may have an entirely different function regarding assembly of Raptor into mTORC1.

2.6 Conclusion

CCT contributes to several important biochemical pathways by folding their components. Structural similarities between Gβ and mLST8 led us to investigate new role of CCT in mTOR pathway as a chaperone for mLST8. Biochemical and signaling experiments confirmed our hypothesis that CCT facilitates folding and assembly of mLST8, thereby contributing to mTOR signaling. During the course of these studies, Raptor was also identified as a novel substrate for CCT and we confirmed that the C-terminal domain of Raptor interacts with CCT. Structural comparison between Gβ-CCT and mLST8-CCT showed that CCT interacts with each substrate in a unique manner, despite their structural similarities. High resolution structural information could be used to design small molecules that interfere in the folding process of mLST8 and hence could have therapeutic implications based on an ability to modulate mTOR signaling.

REFERENCES

1. Yip, C.K., et al., *Structure of the human mTOR complex I and its implications for rapamycin inhibition.* Mol Cell, 2010. **38**(5): p. 768-74.

2. Sarbassov, D.D., et al., *Prolonged rapamycin treatment inhibits mTORC2 assembly and Akt/PKB.* Mol Cell, 2006. **22**(2): p. 159-68.

3. Bentzinger, C.F., et al., *Skeletal Muscle-Specific Ablation of raptor, but Not of rictor, Causes Metabolic Changes and Results in Muscle Dystrophy.* Cell Metabolism, 2008. **8**(5): p. 411-425.

4. Polak, P., et al., *Adipose-specific knockout of raptor results in lean mice with enhanced mitochondrial respiration.* Cell Metabolism, 2008. **8**(5): p 399-410.

5. Arias, E., et al., *Lysosomal mTORC2/PHLPP1/Akt Regulate Chaperone-Mediated Autophagy.* Mol Cell, 2015. 59(2): p. 270-84.

6. Sarbassov DD., et al., *Rictor, a novel binding partner of mTOR, defines a rapamycin-insensitive and raptor-independent pathway that regulates the cytoskeleton.* Curr Biol. 2004 **14**(14): p1296–1302.

7. Betz, C. and M.N. Hall, *Where is mTOR and what is it doing there?* J Cell Biol, 2013. 203(4): p. 563-74.

8. Rosner, M. and M. Hengstschlager, *Cytoplasmic and nuclear distribution of the protein complexes mTORC1 and mTORC2: rapamycin triggers dephosphorylation and delocalization of the mTORC2 components rictor and sin1.* Hum Mol Genet, 2008. 17(19): p. 2934-48.

9. Roberto, Z., et al., *mTOR: from growth signal integration to cancer, diabetes and ageing.* Nature Reviews Molecular Cell Biology, 2011. 12 (12): p. 21-35.

10. Perry, J. and N. Kleckner, The ATRs, ATMs, and TORs are giant HEAT repeat proteins. Cell, 2003. 112(2): p. 151-5.

11. Yang, H., et al., mTOR kinase structure, mechanism and regulation. Nature, 2013. 497(7448): p. 217-23.

12. Guertin, D.A., et al., *Ablation in mice of the mTORC components raptor, rictor, or mLST8 reveals that mTORC2 is required for signaling to Akt-FOXO and PKCalpha, but not S6K1.* Dev Cell, 2006. 11(6): p. 859-71.

13. Kakumoto, K., et al., *mLST8 Promotes mTOR-Mediated Tumor Progression.* PLoS One, 2015. 10(4): p. e0119015.

14. Aylett, C.H., et al., *Architecture of human mTOR complex 1.* Science, 2016. **351**(6268): p. 48-52.

15. Kim, D.H., et al., *mTOR interacts with raptor to form a nutrient-sensitive complex that signals to the cell growth machinery.* Cell, 2002. **110**(2): p. 163-75.

16. Tzatsos, A., *Raptor binds the SAIN (Shc and IRS-1 NPXY binding) domain of insulin receptor substrate-1 (IRS-1) and regulates the phosphorylation of IRS-1 at Ser-636/639 by mTOR.* J Biol Chem, 2009. **284**(34): p. 22525-34.

17. Saxston, R.A., *mTOR Signaling in Growth, Metabolism, and Disease.* Cell, 2017. **168**(6): p. 960-976.

18. Sanack, Y., *PRAS40 Is an Insulin-Regulated Inhibitor of the mTORC1 Protein Kinase.* Molecular Cell, 2017. **25**(6): p. 903-915.

19. Peterson, R.T*., DEPTOR Is an mTOR Inhibitor Frequently Overexpressed in Multiple Myeloma Cells and Required for Their Survival.*Cell, 2009. **137**(5): p. 873-886.

20. Gaubitz, C., et al., *TORC2 Structure and Function.* Trends Biochem Sci, 2016. **41**(6): p. 532-45.

21. Wullschleger, S., et al., *Molecular Organization of Target of Rapamycin Complex 2.* J. Biol. Chem., 2005. **280**(35): p. 30687-30704.

22. Zhou, P., et al., *Defining the Domain Arrangement of the Mammalian Target of Rapamycin Complex Component Rictor Protein.* J. Comp. Biol, 2015. **22**(9): p. 876-886.

23. Cameron J.A., et al., *mTORC2 targets AGC kinases through Sin1-dependent recruitment.* Biochem.J., 2011. **439**: p. 287–297.

24. Harrington, L.S., et al., *TheTSC1-2 tumor suppressor controls insulin-PI3K signaling via regulation ofIRS proteins.* J. Cell Biol., 2004. **166**(2): p.213–223.

25. Inoki, K., et al., *TSC2 is phosphorylated and inhibited by Akt and suppresses mTOR signalling.*Nat Cell Biol., 2002. **4**(9): p.648–657.

26. Ma, L., et al., *Phosphorylation and Functional Inactivation of TSC2 by Erk.* Cell, 2005. **121**(2): p. 179-193.

27. Inoki, K., et al. *TSC2 integrates Wnt and energy signals via a coordinated phosphorylation by AMPK and GSK3 to regulatecell growth*. Cell, 2006.**126**(5): p. 955–968.

28. Brugarolas, J., et al., *Regulation of mTOR function in response to hypoxia by REDD1 and the TSC1/TSC2 tumor suppressor complex.* Genes Dev., 2004. **18**(23): p. 2893–2904.

29. Kim, E., et al.,*Regulationof TORC1 by Rag GTPases in nutrient response.* Nat. Cell Biol., 2008. **10**(8): p.935–945.

30. Zoncu, R., et al., *mTOR: from growth signal integration to cancer, diabetes and ageing.* Nature Reviews. , 2011. **12** p. 21-35.

31. Brunn, G.J., et al., *Phosphorylation of the translational repressor PHAS-I by the mammalian target of rapamycin.* Science.,1997. **277**, p. 99–101.

32. Santro, E.E., et al., *FOXO3a Is a Major Target of Inactivation by PI3K/AKT Signaling in Aggressive Neuroblastoma.* Mol. Cell. Pathobiology., 2013. **73**(7): p 2189-2198.

33. Hsu, P.P., et al., *The mTOR-regulated phosphoproteome reveals a mechanism of mTORC1-mediated inhibition of growth factor signaling.* Science., 2011. **332**(6035): p.1317-1322.

34. Pal, M., et al., *Structural basis for phosphorylation-dependent recruitment of Tel2 to Hsp90 by Pih1.* Structure, 2014. **22**(6): p. 805-18.

35. Takai, H., *Tel2 Regulates the Stability of PI3K-Related Protein Kinases.* Cell., 2007. **131**(7): p. 1248-1259.

36. David-Morrison, G., et al., *WAC Regulates mTOR Activity by Acting as an Adaptor for the TTT and Pontin/Reptin Complexes.* Dev Cell, 2016. **36**(2): p. 139-51.

37. Kim, Y.E., et al., *Molecular chaperone functions in protein folding and proteostasis.* Annu Rev Biochem, 2013. **82**: p. 323-55.

38. Valpuesta, J.M., et al., *Structure and function of a protein folding machine: the eukaryotic cytosolic chaperonin CCT.* FEBS Lett, 2002. **529**(1): p. 11-6.

39. Zhang, J., et al., *Mechanism of folding chamber closure in a group II chaperonin.* Nature, 2010. **463**(7279): p. 379-83

40. Camasses, A., et al., *The CCT chaperonin promotes activation of the anaphase-promoting complex through the generation of functional Cdc20.* Mol Cell, 2003. **12**(1): p. 87-100.

41. Willardson, B.M. and C.M. Tracy, *Chaperone-mediated assembly of G protein complexes.* Subcell Biochem, 2012. **63**: p. 131-53.

42. Feldman, D.E., et al., *Tumorigenic mutations in VHL disrupt folding in vivo by interfering with chaperonin binding.* Mol Cell, 2003. **12**(5): p. 1213-24.

43. Trinidad, A.G., et al., *Interaction of p53 with the CCT complex promotes protein folding and wild-type p53 activity.* Mol Cell, 2013. **50**(6): p. 805-17.

44. Kabir, M.A., et al., *Physiological effects of unassembled chaperonin Cct subunits in the yeast Saccharomyces cerevisiae.* Yeast, 2005. **22**(3): p. 219-39.

45. Behrends, C., et al., *Network organization of the human autophagy system.* Nature, 2010. **466**(7302): p. 68-76.

46. Abe, Y., et al., *p90 ribosomal S6 kinase and p70 ribosomal S6 kinase link phosphorylation of the eukaryotic chaperonin containing TCP-1 to growth factor, insulin, and nutrient signaling.* J Biol Chem, 2009. **284**(22): p. 14939-48.

47. Lukov, G.L., et al., *Phosducin-like protein acts as a molecular chaperone for G protein betagamma dimer assembly.* EMBO J, 2005. **24**(11): p. 1965-75.

48. Lai.,C.W., et al., *Phosducin-like protein 1 is essential for G-protein assembly and signaling in retinal rod photoreceptors.* J. Neurosci., 2013. **33**(18): p. 7941-7951.

49. Tracy., C.M., et al., *Retinal Cone Photoreceptors Require Phosducin-Like Protein 1 for G Protein Complex Assembly and Signaling.* PLoS One., 2015. **10**(2): p e0117129.

50. Plimpton., R.L., et al., *Structures of the Gβ-CCT and PhLP1-Gβ-CCT complexes reveal a mechanism for G-protein β-subunit folding and Gβγ dimer assembly.* PNAS., 2015. **112**(8): p.2413-2418.